INTERPRETATION OF THE AEROMAGNETIC ANOMALIES CVER THE YOUNGER GRANITES OF JOS-PANKSHIN AREA IN PLATEAU STAIE, NIGERIA

BY

ROLAND KANGKOLO

SUBMITTED IN PARTIAL FULFILLEMNT OF THE REQUIREMENTS FOR THE DEGREE OF MASTER OF SCIENCE, APPLIED GEOPHYSICS.

DEPARTMENT

OF PHYSICS

AHMADU EELLO UNIVERSITY
ZARIA-NIGERIA. . . . . ,

OCTOEER, 1 9 8 4

DECLARATION

This thesis is an original work carried out by the author under the supervision of Professor D.E. Ajakaiye, Head of Department of Physics and Dr. M.B. Awad, M.Sc. Geophysics Course Co-ordinator.

To the best of my knowledge, no part thereof has been submitted elsewhere for the award of a degree or diploma. The work of others is duly acknowledged and referenced.

Author

Supervisor

A.B.U. Zaria

OCTOBER, 1984

ABSTRACT

A prepared residual magnetic field map of the central part of Jos Plateau revealed that most of . the significant magnetic anomalies correlate with known geological features However, at least seven prominent anomalies could not be correlated with any exposed geological features, These anomalies were attributed to be buried structures.

Quantitative three-dimensional magnetic interpretation of four of the uncorrelated anomalies were made. The models obtained indicate that the anomalies arise from bodies of negative susceptibility contrast (-0.00078 emu to -0.00425 emu) with respeet to the basement; most of these bodies were flanked by other bodies with positive susceptibility contrasts (+0,000625 emu to +0.00152 emu). Values of the susceptibility contrast (-0.00078 emu to -0.00425 emu) indicate the former bodies as being Younger Granite rock-types and the latter as being basalts or basic rocks.

The buried structures in the eastern half of the area and some of the exposed Younger Granite massifs form NNW alignments which are parallel to structural tends in the basement complex in this region.

The models indicate that the buried structures are located at an average depth of 1km below the surface, extend to between 3km and 14km, and have near-vertical sides and polygonal cross-sections. These shapes conform with the concept of the origin of Younger Granites from cauldron subsidence in magma chambers within the crust.

ACKNOWLEDGEMENT

At the successful completion of this work, I would like to express my sincere thanks to Professor D.E. Ajakaiye, Head of Physics Department, Ahmadu Bello University, Zaria for suggesting the project, for her supervision, and for the inspiration and very useful assistance during this work.

I am deeply indebted to my supervisor Dr. M.B. Awad for his invaluable guidance, keen interest and the advice which he readily gave at all times during my project work and the writing of this report.

Also, I wish to express my appreciation to my friends, and the Geophysics Staff of Ahmadu Bello University, Zaria who by way of useful discussions and otherwise, have contributed to the success of this work.

Finally, I am very thankful to the Society of Exploration Geophysicists (SEG) of America for their award which helped to relieve my financial burden.

TABLE OF CONTENTS

	PAGE
ABSTRACT.....	iii
ACKNOWLEDGEMENTS..	v
TABLE OF CONTENTS.....	vi
LIST OF TABLES.....	viii
LIST OF FIGURES.....	ix
LIST OF SYMBOLS.....	x
CHAPTER 1 - INTRODUCTION.....	1
1.1 GENERAL	1
1.2 THE MAGNETIC PROSPECTING METHOD.....	1
1.3 LOCATION OF THE AREA.....	3
1.4 PREVIOUS GEOPHYSICAL WORK ON THE AREA OF STUDY.....	4
1.5 AIM OF WORK.....	7
CHAPTER 2 - GEOLOGY.....	10
2.1 GENERAL.....	10
2.2 THE BASEMENT COMPLEX.....	10
2.3 THE YOUNGER GRANITES.....	13
2.3.1 Biotite Granites.....	16
2.3.2 Rhyolites.....	18
2.3.3 Hornblende-Granite and Porphyries....	18
2.3.4 Riebeckite - Granites.....	19
2.3.5 Syenites and Basic Rocks.....	19
2.4 THE BASALTS.....	20
CHAPTER 3 - THEORY OF THE MAGNETIC METHOD....	22
3.1 FOUNDAMENTAL THEORY.....	25
3.2 SOURCES OF MAGNETIC ANOMALIES.....	29

CONTENTS (contd.)

CHAPTER 4 - DATA ANALYSIS (REDUCTION)..... 34
4.1 PRELIMINARIES 34
4.2 STATISTICAL ANALYSIS OF RESID UAL FIELD AND GEOLOGICAL FEATURES..... 37
4.3 MODELLING..... 41
4.3.1 Initial Values Of Body Parameters..... 41
4.3.2 3-Dimensional Magnetic Modelling..... 44
CHAPTER 5 - INTERPRETATION..... 47
5.1 MODELLING OF ANOMALY NO. 2..... 47
5.2 MODELLING OF ANOMALY NO. 3..... 54
5.3 MODELLING OF ANOMALY NO. 4..... 60
5.4 MODELLING OF ANOMALY NO. 5..... 66
5.5 DEDUCTIONS FROM THE MODELS..... 71
CHAPTER 6 - CONCLUSION..... 73
6.1 SUMMARY AND DISCUSSIONS..... 73
6.2 SUGGESTIONS FOR FURTHER WORK..... 77
APPENDIX 1..... 79
APPENDIX 2..... 85
REFERENCES..... 90

LIST OF TABLES

TABLE NO.	TITLE	PAGE
2.1	Rocks of the Younger Granite Province	12
2.2	Area and composition of the Younger Granite Complexes	15
3.1	Magnetic Units in SI and Cgs Systems	25
4.1	Properties of Distinct Magnetic Anomalies in Area of Study	36
4.2	Location of anomalies arising from burried Younger Granites	38
4.3	Elementary Statistical Quanties for the Anomalies occuring over various rock-types	42
4.4	Average Magnetic Susceptibilities of Rocks of the Younger Granite Province	43
5.1	Parameters of Modelled Bodies For Anomaly No. 2	51
5.2	Parameters of Modelled Bodies For Anomaly No. 3	57
5.3	Parameters of Modelled Bodies for Anomaly No. 4	63
5.4	Parameters of Modelled Bodies for Anomaly No. 5	68

LIST OF FITURES

FIG. NO.	TITLE	PAGE
1.1	Simplified Geological Map Of Nigeria showing Location of the Nigerian Younger Granite Province	5
2.1	Geology of the Central Younger Granite Province	11
3.1	Components of the Magnetic Field Vector	23
3.2	Relation Between Magnetization (M) and Magnetic Field Intensity for a magnetic mineral	31
4.1	Location of Anomalies suspected to be due to Burried Younger Granites	39
4.2	Idealized Magnetic Profiles for depth estimation by half-slope method	45
5.1	Field of Anomaly No. 2	48
5.2	Profiles through Anomaly No. 2	49
5.3	Modelled Bodies of Anomaly No. 2	52
5.4	Calculated Fields for Anomaly No. 2	53
5.5	Field of Anomaly No. 3	55
5.6	Profile through Anomaly No. 3	56
5.7	Calculated Fields for Anomaly No. 3	58
5.8	Modelled Bodies of Anomaly No. 3	59
5.9	Fields of Anomaly No. 4 and No. 5	61
5.10	Profile through Anomaly No. 4	62
5.11	Calculated Fields for Anomaly No. 4	64
5.12	Modelled Bodies of Anomaly No. 4	65
5.13	Profile through Anomaly No. 5	67
5.14	Calculated Fields for Anomaly No. 5	69
5.15	Modelled Bodies of Anomaly No. 5	70

LIST OF SYMBOLS

SYMBOL	MEANING
nT	nano- Tesla
cgs	centimetre-gramme-second (system of units)
SI	international system
emu	electromagnetic units
s	second
m	meter
km	kilometre
N	north
E	east
W	west
S	south

CHAPTER 1

INTRODUCTION

1.1 GENERAL

The aim of geophysics is to define the geometry and composition of subsurface structures by using physical measurements taken at the surface.

Geophysical methods that have been developed have exploited the possession by the earth's core, mantle and crust of some intrinsic physical properties such as the generation of heat, and magnetic and gravitational fields. There is also the response of the subsurface to seismic and electromagnetic waves, some of which may be artificially generated.

1.2 THE MAGNETIC PROSPECTING METHOD

The magnetic method makes use of the magnetic field generated by the earth. Rock bodies possess magnetic properties, and so they can be detected by the anomalies that they produce on the earth's field. The map of the earth's magnetic field over an area represents a super-position of two largely separate anomally systems. The regional field consists of broad anomalies which arise from magnetic rocks deep in the earth's crust, or from a very broad dispersion of magnetization nearer to the surface. The second is the local field, which consist of narrow anomalies caused by relatively near-surface formations or structures.

The form of the magnetic anomaly from a given body depends on the following factors:-

i. The geometry of the body,

ii. the direction of the earth's field at the location of the body,

iii. the direction of polarization of the rocks forming the body,

iv. the orientation of the body with respect to the direction of the earth's field,

v. the orientation of the line of observation (flight line for aeromagnetic data) with respect to the axis of the body.

Magnetic surveys are mainly applied in three ways. The most obvious is in the search for magnetite. The second application is when the mineral being sought is not magnetic but has magnetite or pyrrhotite associated with it. The third is based on the fact that most mafic igneous rocks and some chemical sediments contain sufficient magnetite to make them sources of magnetic anomalies. Therefore, magnetic surveys offer a quick method of mapping underground structures. This is important in the search for water, oil, gas, etc. Structural information of importance in engineering applications can also be derived from magnetic surveys. Magnetic surveys may be carried out by aircraft, by boat (or ship), or on the ground by foot or road transport. The

study presented in this thesis is the result of an airborne (aeromagnetic) survey.

The first step in the interpretation of aeromagnetic surveys is qualitative, with the goal of detecting such characteristics as anomaly distributions and structural trends. The construction of residual maps is one of the best known ways of studying a magnetic contour map quantitatively. The residual procedures are designed to separate broad regional variations from sharper local anomalies. In effect, the map is split into two parts, the residual and the regional maps. Depending on the goals of interpretation, the anomaly field can be continued upward or downward. The second vertical derivative or curvature of the magnetic field is another function often computed from the total intensity maps. This derivative emphasizes the effects of sharp local anomalies at the expense of the broader regional features.

1.3 LOCATION OF THE AREA

The Jos Plateau is part of the area occupied by the Nigerian Younger Granite Complexes (Fig. 1.1). The latter are grouped in north-central Nigeria covering a distance of about 350km from the Benue Valley in the south to Kano State in the North. The Younger Granites present the topographic distinctiveness of rocky hill massifs, which can

be sharply differentiated from the smoother topography of the surrounding basement rocks. They are generally uplifted to an altitude of the order of 700m above the surrounding terrain.

The area on which this work is focussed lies in the central part of the Nigerian Younger Granite Province, extending from latitude $9^{o}00'$ in the south to $10^{o}00'$ in the north; and from longitude $8^{o}30'$ in the west to longitude $9^{o}30'$ in the east. The area is mapped on 1:100 000 aeromagnetic and geological sheets: 168, 169, 189 and 190, named Naraguta, Maijuju, Kurra and Pankshin respectively.

1.4 PREVIOUS GEOPHYSICAL WORK ON THE AREA OF STUDY

The first geophysical work carried out in the Younger Granite Province was in search of cassiterite, columbite, and other mineral deposits. These had been found to occur in burried river channels or deep leads which are cut into bed-rock and subsequently filled with alluvial and/or volcanic material. Electrical resistivity methods and magnetic methods have been used to locate these buried channels, thus enabling a reduction in the amount of exploratory drilling in the search for tin (Deprees, 1948; Shaw, 1951).

One aeromagnetic map (sheet 168 Naraguta) of a limited part of the province was published in 1963 by Canadian Aero Service Limited under a Canadian

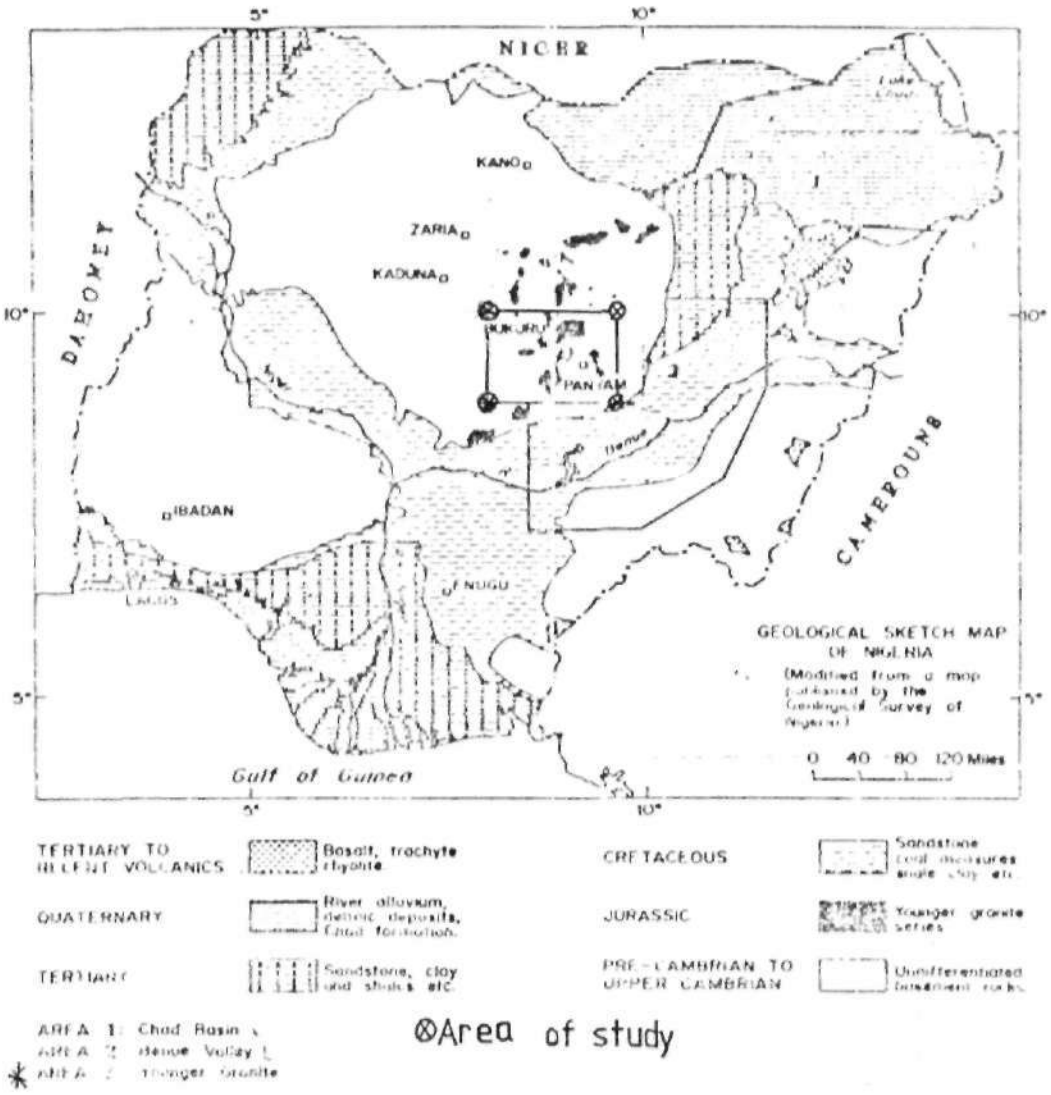


FIG 1·1

SIMPLIFIED GEOLOGICAL MAP OF NIGERIA SHOWING THE NIGERIAN YOUNGER GRANITE PROVINCE

(Adapted from Ajakaiye , 1974)

Technical Assistance Programme in Nigeria. As a follow-up of this work, a comprehensive geophysical study of the area (about 350km^2) was carried out in 1964 to 1965 under the auspices of the United Nations Mineral Project and the British Overseas Geological Surveys. Magnetic, Seismic, resistivity and gravity techniques were used in search of basalt-covered alluvial cassiterite (Masson-Smith, 1965).

This was followed by largely isolated but detailed gravity, magnetic, heat-flow and resistivity surveys carried out in the area (Masson-Smith, 1965; Ajakaiye, 1968; Ajakaiye et al, 1975; Verheijen and Ajakaiye, 1980). Some of the surveys have resulted in the location of new deposits in the vicinity of the complexes (Ajakaiye, 1974).

Then followed a reconnaissance gravity survey of the area undertaken to shed light on the form and shape of the Younger Granite ring-complexes at depth, on the origin of the ring-complexes, and to discover any unexposed and hitherto unknown ring-complexes in the province (Ajakaiye, 1970, 1975, 1976).

Closely connected with this was the determination of the densities of rocks of the Younger Granite Province carried out by Ajakaiye between 1970 and 1972. The density determinations involved rocks collected from various Younger Granite outcrops

located all over the province. The findings have since been very useful in subsequent gravity interpretations.

The gravity method was successful in providing information about the deep structural features of the area due to the density contrast of 0.6×10^{3} kg. m^{-3} between the rocks of the surrounding crystalline basement and those of the Younger Granites.

A recent study of aeromagnetic anomalies across the Nigerian Younger Granite Province carried out by Ajakaiye et al (1982) revealed the trends and lineaments of the Younger Granite ring-complexes indicating a relationship between these and structural features of the Benue Trough. It also related rock-types with characteristic magnetic anomaly values. Further, a quantitative interpretation permitted a geometric definition of many of the prominent Younger Granite ring-complexes.

1.5 AIM OF WORK

In a detailed Gravity survey of the Younger Granite Province carried out by Ajakaiye in 1974, the presence of unexposed Younger Granite intrusions was indicated north of Banke and Liruei. Recent studies of aeromagnetic anomalies of the Younger Granite Province (Ajakaiye et al, 1982) have also revealed some anomalies believed to be due to unexposed Younger Granite intrusions buried at

relatively shallow depth.

The work presented here is a follow-up of the above. The objectives are:-

i. To locate some of the areas with buried Younger Granite intrusions, and then to carry out quantitative interpretations of the aeromagnetic anomalies over such areas with a view to obtaining information on the properties of the buried structures giving rise to the anomalies.

ii. To provide an opportunity for examining some postulated theories on the tectonic origin, structural evolution, geochemistry, etc. of the Younger Granite complexes.

iii. To investigate the structural and petrological similarities between exposed and unexposed Younger Granite complexes.

iv. To obtain indications on the mode of emplacement of the unexposed structures from their geometric outlines. For example: bodies which have resulted from subsidence of blocks bounded by intersecting ring-fractures of different radii of curvature, will take the form of elliptical and crescentic intrusions of limited arcuate extent. On the other hand, structures occupying open circular and polygonal

fractures would have resulted from persistent upward pressure by the underlying magma giving rise to doming and distension of roof-rocks under tensional conditions (W.N. MacLeod and D.C. Turner, 1965).

CHAPTER 2

GEOLOGY

2.1 GENERAL

The geological sequence in the Younger Granite Province is made up almost entirely of plutonic and volcanic rocks belonging to four main age groups. Sediments are restricted to valley alluvium. A generalized succession is presented in Table 2.1.

Much of the area is underlain by rocks of the basement complex. The oldest recognized include granulitic gneisses in small, widely scattered outcrops and a few small bodies of dioritic rocks. The rest of the basement complex consists of rocks of a single orogenic cycle. The Province is geologically dominated by the Younger Granites, a series of non-orogenic intrusives and associated acid volcanics (Fig. 2.1).

2.2 THE BASEMENT COMPLEX

Basement rocks which comprise of a complex series of migmatites and granites make up more than two-thirds of the Younger Granite Province. The older Granites and accompanying metamorphism of the basement are dated at about 500 to 600 million years, and represent the Pan-African orogeny in Nigeria (Jacobson et al, 1964; Van Breeman and Bowden, 1973).



FIG 2·1

GEOLOGY OF THE CENTRAL YOUNGER GRANITE PROVINCE

(From Ajakaiye et al, 1982)

TABLE 2.1: ROCKS OF THE YOUNGER GRANITE PROVINCE

AGE	ROCK GROUPS	ROCK TYPES
Quaternary	Newer Basalts	Lava flows and Volcanic cones
Tertiary Quarternary	Alluvium	
Lower Tertiary	Older Basalts	Lava flows, now largely decomposed, overlying alluvium (formerly termed Fluvio-volcanic series)
Jurassic	Younger Granites	Granites, Porphyries and Rhyolites
Pre-Cambrian to Lower Palaeozoic	Crystalline Basement	Migmatites, gneisses and Older Granites

(ADAPTED FROM WRIGHT, 1965)

The general sequence of rock-types consists of a group of older granulitic gneisses succeeded by a series of migmatites, granite-gneisses, and granites. These form a single petrogenic sequence which can be classified under the groups: Pre-migmatitic rocks (including intermediate rocks), Migmatites, Granite-gneiss (and migmatitic granite-gneiss), older Granites (Wright, 1965).

The dominant foliation in the basement and the direction of elongation of many of the granite masses is north-south which is parallel to the trend in basement areas further to the west.

2.3 THE YOUNGER GRANITES

The Younger Granites are discordant, high-level intrusions which transgress all units of the basement complex (Turner and MacLeod, 1965). They have been emplaced by ring-faulting and block-subsidence. Intermediate and basic rocks occur in many of the complexes, but most of the syenites are quartz-bearing. The gabbros, micro-gabbros and dolerites occupy less than one per cent of the total area and comprise only a minor part of any complex in which they occur. Granites as the main rocks have been classified on the basis of the dominant minerals:
(1) hornblende-pyroxene-fayalite-granites,
(2) biotite-granites, (3) riebeckite-granites.

Nearly fifty Younger Granite massifs are known, varying greatly in size, many of the larger ones being made up of two or more overlapping ring complexes. They occur in a broad north-south zone, 400 x 150 km, centred on the Jos Plateau where the greatest concentration of the ring complexes is found.

The emplacement of the Younger Granites is completely unrelated to orogenic activity. Their age is Jurassic, around 150 to 170 million years. However, it seems likely that emplacement of the Younger Granites was associated with epeirogenic uplift. Indirect evidence for this is the lack of sediments associated with the volcanic rocks of Younger Granite age, which were apparently erupted onto a land surface undergoing erosion, not deposition (Turner, 1974).

The basement rocks appear to have exerted some control over Younger Granite emplacement. Structurally, the generally north-south trend of the basement rocks may have influenced the north-south form of the Younger Granite intrusive belt. On a more detailed scale also, structures in the basement appear to have influenced the location of the Younger Granite ring complexes. The Jos Plateau lies in a discontinuity in the basement; to the west the structural trend is north-south but to the east it is northeast-southwest and east-west.

TABLE 2.2: AREAS (km^2) AND COMPOSITION OF THE YOUNGER GRANITE COMPLEXES

COMPLEX	ROCK TYPE							TOTAL
	R_1	R_2	R_3	R_4	R_5	R_6	R_7	
C1	135.7	52.1	2.1	13.2	40.9	1.8	6.5	252.3
C2	17.9	25.9	-	47.7	37.0	-	-	128.5
C3	-	-	-	9.6	2.1	-	-	11.7
C4	8.5	4.7	-	43.3	21.0	22.3	-	99.7
C5	-	3.6	3.4	183.6	-	-	-	190.6
C6	0.5	-	-	-	-	-	-	0.5
C7	0.3	2.3	-	0.3	-	-	-	2.8
C8	-	-	6.7	97.9	14.5	-	-	119.1
C9	18.9	7.5	-	21.8	3.9	-	-	52.1
C10	-	-	0.8	5.2	-	-	5.7	11.7
C11	-	-	1.3	98.9	-	-	-	100.2
C12	-	-	-	10.9	-	-	-	10.9
C13	72.5	52.3	215.7	734.0	21.2	-	1.3	1097.1
C14	-	-	-	0.3	-	-	-	0.3
C15	-	10.9	114.2	46.1	22.0	-	-	193.2
C16	-	-	-	11.9	-	-	-	11.9
C17	-	22.0	41.7	6.7	-	-	-	70.4
C18	2.8	28.2	32.4	83.7	19.9	-	-	167.1
C19	1.3	36.8	149.7	124.3	12.4	7.3	4.4	336.2
C20	-	0.5	-	28.7	-	-	-	29.3
C21	43.0	26.4	148.1	374.8	-	6.5	10.4	609.2
C22	-	-	-	3.4	-	-	-	3.4
TOTAL	301.5	273.2	716.1	1946.1	195.0	37.8	28.2	3498.1

R1 : Rhyolite

R2 : Hornblende-fayalite-Granite and Porphyry

R3 : Hornblende-biotite-granite

R4 : Biotite-granite

R5 : Riebeckite- and riebeckite-biotite-granite

R6 : Syenite R7 : Gabbro, dolerite, etc.

C1 : Saiya-Shokobo C8 : Amo C17 : Kagoro

C2 : Tongolo C9 : Buji C18 : Rop

C3 : Junguru C10: Kofai C19 : Sara-Fier, Pankshin

C4 : Jere-Sanga C11: Rubuka C20 : N

C5 : Kwandonkaya C12: Miango C20 : Ningishi

C6 : Kunkur C13: Jos-Bukuru, Jarawa C21 : Sha-Kaleri, Monguna, Tof

C7 : Satumi C14: Shona C22 : Sharwai

C15: Ganawuri-Kigom

(Adapted from MacLeod & Turner, 1971)

The clearest example of basement control is seen in the north-northwest and north-northeast alignments parallel to zones of shearing in the basement. Other directions of ring complex alignment correspond to basement joints and fractures. It seems probable that such fractures guided the location of the volcanic eruptions initiating each complex (Turner, 1974).

The subdivisions of Younger Granite rock-types can be made on the basis of coloured mineral content, which are quite well-defined. The essential unity and the sub-volcanic nature of the whole suite are emphasized by the gradation from originally glassy rhyolites, through porphyries to coarse-grained granites. The areal extent of the main rock-types is presented on Table 2.2.

2.3.1. BIOTITE-GRANITES

It can be seen from Table 2.2 that with an area of 1,946.1km^2 (55.6 per cent of the total area) biotite-granite is clearly the most abundant and widespread rock-type in the Younger Granite Province, forming some of the largest individual intrusions. The biotite granites are divided into three groups whose typical examples are intrusions of the Jos-Bukuru complex. The first group is made up of coarse-grained biotite-granites, generally pink in

colour and with very widely spaced jointing. The second group consists of medium grained granites, pinkish in colour and grading into the white, even-textured, medium-grained granites. The last group is highly distinctive with biotite growing in separate flakes rather than clusters (MacLeod and Turner, 1971).

The economic tin mineralization in the Province is almost entirely confined to the biotite-granites. The most abundant tin ore is cassiterite which often occurs as alluvial concentrations, shed from the Younger Granite massifs. The cassiterite is sometimes dispersed in multitudinous, narrow greisien veins, and quartz shringers in the roof-zones of the biotite-granite intrusions (Turner, 1971).

Next in importance is columbite which is also a tin ore. The columbite of the Younger Granite Province has the unique mode of occurence as an accessory constituent of the biotite granites. The other economic minerals are of marginal importance. They include: Wolfram, Pyrochlore (a source of niobium), fergusonite (an yrrtrium oxide containing moderate proportions of uranium and thorium), thorite and zircon (sources of thorium and haffnium), monazite (source of thoria), xenotime (rich in rare earths of high atomic number), molybdenite, cryolite, and piezoelectric quartz (Turner, 1971).

2.3.2. RHYOLITES

The rhyolites of the Younger Granite Province are characterized by their division into two distinct sections: the early rhyolites and the late rhyolites. The early rhyolites and the associated fragmented rocks are the products of vent eruptions and the vents have been localized by the initial major ring-fractures which formed at the outset of the Younger Granite magmatic cycle. The late rhyolites are considered to be the products of wholesale surface or shallow subsurface cauldron subsidence and may be either intrusive or extrusive in nature (Turner, 1971).

2.3.3. HORNBLENDE-GRANITES AND PORPHYRIES

Although this group of rocks constitutes only 7.8 per cent of the Younger Granite complexes in this region (Table 2.2), it is important in that it forms the conspicuous ring-dykes of the province. They sometimes appear as large plutons with a truly granitic texture. In the ring-dykes they commonly assume a porphyritic texture, and hence it often referred to as granite-porphyry. Another sub-group is the quartz-fayalite porphyries which occur as the last stage in the volcanic phase of activity and are texturally transitional between the micro-crystalline cauldron rhyolites and the granite

porphyries. The hornblende-biotite-granites form another sub-group consisting of coarse-grained granites occuring as massive ring-dykes or plutons which are restricted to the southern part of the province (MacLeod and Turner, 1971).

2.3.4 RIEBECKITE-GRANITES

This rock-type is of a small areal extent though it appears in the majority of the Younger Granite complexes (Table 2.2). It is most abundant in the northern complexes, and on passing southwards there is a smaller proportion of riebeckite-granite compared to other granites. In northern extension of the province into Niger Republic the proportion of riebeckite-granites is greatly increased (Black, 1965).

2.3.5. SYENITES AND BASIC ROCKS

Both of these rock-types have a small areal spread - collectively occupying about two percent of the Younger Granite Province. The syenites mostly occur in the north-eastern corner of the province, and there are smaller intrusions in about a dozen other complexes. The syenites have a close affinity to the hornblende-fayalite-granites and have granular and porphyritic textures.

The basic rocks are mainly gabbros, dolerites and diorites. Together with basalts, the basic

rocks often occur as lava flows, dykes and semi-concordant intrusions in the rhyolites and granites of many of the complexes, and around the margins of the massifs it is common to find swarms of basic dykes.

2.4 THE BASALTS

The basalts are the most recent rocks in the area. They have resulted from the late Tertiary and Quaternary Volcanism in Nigeria, which can be broadly regarded as part of the Gulf of Guinea volcanic province. The basalts are subdivided into three groups: Lateritized Basalts, Older Basalt and Newer Basalt (Wright, 1968; Grant et al, 1972).

The lateritized Basalts represents lavas now decomposed to clays and usually overlain by a thick cap of lateritic ironstone. They have been recently divided into two groups: an older group consisting of smaller eroded remnants, and a new group consisting of larger valley - filling flows which can be traced to well-preserved cones.

The older and newer Basalts cannot be distinguished from each other petrographically as both groups show a similar variety of rock-types. The older Basalts are generally small, eroded and partly decomposed remnants, lacking a well defined

volcanic focus. While the Newer Basalts occur as lava flows which can be traced to youthful-looking cones little affected by erosion. The cones are mainly built of basaltic scoria and pyroclastics, including many fine volcanic bombs, and have erupted a variety of inclusions (Turner, 1971).

CHAPTER 3

THEORY OF THE MAGNETIC METHOD

The magnetic method is one of the potential methods applied in geophysical prospection. The theoretical basis of the method has been developed using the general mathematical potential theory. Magnetic interpretation involves the inverse problem of finding the manner of distribution of magnetized material whose magnetic field would be identical to the field measured on the surface. This tool has the drawback that from the theoretical standpoint, many combinations of geometric configuration and magnetization can produce the same magnetic field on the surface. Much of this ambiguity can be removed by geological controls and independent sources.

The geomagnetic field is a vector quantity which possesses a definite direction at each point. The vector is often represented as passing diagonally from the origin to the far corner of a rectangular parallepiped (Fig. 3.1). The various magnetic elements are:

T - total intensity; the magnitude of the vector field.

X, Y, Z - North, east and vertical components, respectively, of the magnetic field.

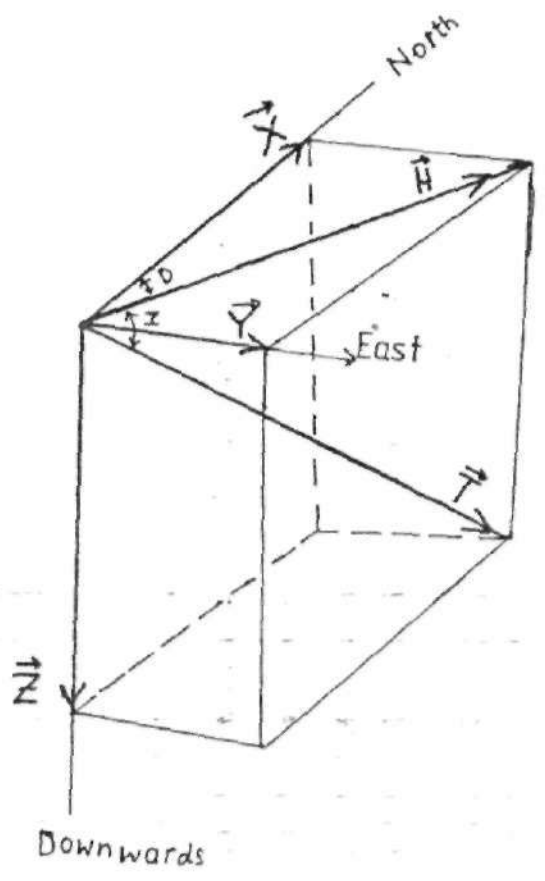


FIG 3·1

COMPONENTS OF THE MAGNETIC FIELD VECTOR

H - Horizontal component of the total field.

I - Inclination or angle of dip of the total intensity vector below the horizontal plane.

D - Declination; angle between H and true North.

The component of interest in this study is the total intensity T, being the component measured in airborne prospecting.

The field at a given place and time may be considered as being made up of three parts:

i. a relatively large, slowly changing, secular part (main field) caused by the earth as a simple, not quite uniformly polarized sphere,

ii. a relatively small diurnal part, which changes somewhat erratically with time but is repeated approximately in daily cycles and may have relatively strong short-term disturbances due to magnetic storms.

iii. Minor variations in the field from place to place which are caused by magnetic inhomogeneities of the earth's crust. This is the part that is of primary interest in magnetic prospecting, and it is commonly referred to as the local field or the anomaly part of the field.

Magnetic quantities are measured in SI or Cgs systems of units. A comparison of the various

magnetic units in SI & Cgs (emu) systems is given on Table 3.1. The adoption of the International System (SI) of units in Physics and engineering has engendered some confusion in magnetism partly because the shift from cgs to SI units requires modifications in some fundamental definitions.

3.1 FUNDAMENTAL THEORY

Fundamentally a region is said to be permeated by a magnetic field if a magnet experiences a torque when placed at the point. Oersted (1800) discovered that a magnetic field always exists in the vicinity of an electric current.

TABLE 3.1

MAGNETIC UNITS IN SI AND Cgs SYSTEMS

QUANTITY	SI (MKSA SYSTEM)	cgs SYSTEM
Magnetic Induction (B)	1 tesla $= 10^9$ nT	$= 10^4$ gauss $= 10^9$ gamma
Magnetic field Intensity (H)	1 amp m^{-1}	$= 4 \times 10^3$ Oersted 1257 gamma
Magnetization (M)	1 amp m^{-1}	$= 10^{-3}$ emu (no special name)
Magnetic Moment (m)	1 amp m^2	$= 10^3$ emu
Magnetic Potential	1 tesla	$= 10^6$ gilberts
Magnetic flux (O)	1 Weber	$= 10^8$ maxwell
Magnetic Susceptibility	Dimension-less K_{SI}	Dimensionless $= 4 \quad k_{cgs}$

(adapted from Parkinson, 1982)

Ampere (1825) showed that a circuit S_1 carrying a current I_1 will in vacuo exert on circuit S_2 carrying a current I_2 a force $\vec{F}$ given by:

$$\vec{F} = \frac{(\mu_o)}{4} I_1 I_2 \oint\oint \vec{ds}_1 \times \frac{(\vec{ds}_2 \times \vec{r})}{r^3} \quad \ldots\ldots\ldots (3.1)$$

where $\vec{r}$ is the position vector of ds_1 relative to ds_2.

The magnetic effect is often expressed in terms of two vectors depending on the role of the constant μ_o. The vectors are: $\vec{H}$ (the magnetic field intensity) and $\vec{B}$ (the magnetic induction). Using H the force between currents can be written as:

$$\vec{F} = \mu_o I_1 \oint \vec{ds}_1 \times \vec{H} \quad \ldots\ldots\ldots\ldots\ldots (3.2)$$

where $\vec{H} = \frac{1}{4}\pi I_2 \oint \frac{\vec{ds}_2 \times \vec{r}}{r^3} \quad \ldots\ldots\ldots\ldots (3.3)$

Using $\vec{B}$ we get; $\vec{F} = I_1 \oint \vec{ds}_1 \times \vec{B} \ldots\ldots\ldots\ldots (3.4)$

with $\vec{B} = (\mu_o/4)\ I_2 \oint \frac{\vec{ds}_2 \times \vec{r}}{r^3} \quad \ldots\ldots\ldots (3.5)$

These relations apply in a vacuum, or in the absence of a magnetic material. If a magnetic material is present the effect of the material must be taken into account. Thus H is defined so that (3.3) still applies and an extra vector must be added to (3.2) which now becomes:

$$\vec{F} = \mu_o I \oint \vec{ds} \times (\vec{H} + \vec{M}) \ldots\ldots\ldots\ldots (3.6)$$

where $\vec{M}$ is the magnetization vector. $\vec{B}$ is defined so that (3.4) still applies.

Therefore, the relation between $\vec{B}$, $\vec{H}$ and $\vec{M}$ is

$$\vec{B} = \mu_o(\vec{H} + \vec{M}) \quad \ldots\ldots\ldots\ldots\ldots\ldots (3.7)$$

For some mineral $\vec{M}$ is proportional to and parallel to $\vec{H}$ and can be expressed:

$$\vec{M} = k\,\vec{H} \quad \ldots\ldots\ldots\ldots\ldots\ldots\ldots\ldots (3.8)$$

The scalar k is called the 'magnetic susceptibility' of the material. Then for such material we can write:

$$\vec{B} = \mu_o\,(\vec{H} + k\vec{H}) = \mu_o\,(1 + k)\,\vec{H}$$

$$\vec{B} = \mu\vec{H} \quad \ldots\ldots\ldots\ldots\ldots\ldots\ldots\ldots (3.9)$$

where $\mu = \mu_o\,(1 + k)$ $\ldots\ldots\ldots\ldots\ldots\ldots (3.10)$

is known as the magnetic permeability of the material. μ_o is the permeability of a vacuum, or of non-magnetic material.

The magnetic state of a body can be thought of as arising from elementary magnets or dipoles which interact with each other through their magnetic fields. An important property of the dipole is its moment (M): the torque experienced when the dipole is set with its axis at right angles to a magnetic field of unit size.

The magnetic field intensity at a point, distance r from the dipole, is the force per unit pole strength exerted by the dipole at that point.

$$\vec{H}(r) = \frac{2m\cos\theta}{r^3}\vec{U}r + \frac{m\sin\theta}{r^3}\vec{U}o \quad \ldots\ldots (3.11)$$

where θ is the angle measured from M to r, and $\vec{U}r$, and $\vec{U}o$ are unit vectors in direction of r and θ respectively.

Being a force field, the magnetic field is derivable from a scalar potential designated A(r):

$$\vec{H}(r) = -\nabla A(\vec{r}) \quad \ldots\ldots\ldots\ldots\ldots\ldots\ldots (3.12)$$

where $A(\vec{r}) = \frac{m\cos\theta}{r^2} = -\vec{m}.\ \nabla\ (1/r)$

Assuming a continuous distribution of magnetic moment within a magnetic body, the magnetic moment per unit volume at a point in the body r_o from an origin (also within the body) is designated $\vec{M}(r_o)$.

The magnetic scalar potential at a point outside the body (volume v) can be obtained by intergrating over the volume of the body:

$$A(\vec{r}) = -\int_v M\ (r_o).\ \nabla\ (1/|r-r_o/dv \quad \ldots\ldots (3.13)$$

Substituting in (3.12) gives the magnetic field intensity at this point as:

$$H(r) = \nabla\int_v M.\ \nabla\ 1/|\ r-ro/dv \quad \ldots\ldots\ldots\ldots (3.14)$$

Outside the body the intergral in (3.13) is now singular and $A(\vec{r})$ satisfies Laplace's equation:

$$\nabla 2A = 0.$$

Inside the body the integral becomes singular at r = ro. To isolate the singularity, we enclose it within a small (3.13) can be written:

$$A(r) = -\int_{V-V'} M(r_o).\nabla\frac{dv}{r-ro} - \int_{V} M(r).\nabla\left(\frac{1}{|r-r|}\right) dV$$

The first term is non singular and is harmonic everywhere. It will vanish when the Laplican of A(r) is taken.

$$\therefore \quad \nabla^2 A(r) = -\nabla.\nabla\left[\int_{V'} \vec{M}(ro).\nabla\left(\frac{1}{|r-ro|}\right) dv\right].$$

By making ϵ small enough M(ro) can be regarded as a constant and thus:

$$\nabla^2 A(r) = -\nabla. M(r)\int_{V'} \nabla.\nabla\left(\frac{1}{|r-ro|}\right) dv.$$

Applying Causs' theorem we change the volume integral into a surface intergral over the sphere of radius ϵ.

$$\nabla^2 A(r) = -\nabla .M(r)\int_S \vec{n} .\nabla\frac{1}{|r-ro|} ds$$

where $|r-ro| = \epsilon$, $n.v = \frac{\partial}{\partial\epsilon}$ and $\vec{n}$ is unit vector normal to the surface.

$$\nabla^2 A(r) = -\nabla.\vec{M}(r)\int_S \frac{\partial}{\partial\epsilon}\ (1/\epsilon)\ ds$$

In the limit as $\epsilon \to o$,

$$\nabla^2 A(r) = -\nabla.M.(r)\ \left(\frac{d}{d\epsilon}\ 1/\epsilon\right)\int_S ds = -\nabla.M(r)\text{--}$$

$$(-1/\epsilon)4\pi E^2$$

$$\nabla^2 A(r) = 4\pi\nabla.M(ro) \qquad (3.15)$$

The magnetic potential satisfies Poisson's equations anywhere inside a magnetic body.

3.2 SOURCES OF MAGNETIC ANOMALIES

Magnetization of a rock is of two kinds: induced magnetization and remanent magnetization. Induced

magnetization is that part of the rock magnetism which is proportional to the ambient field. This is the more significant part in that while there are many exceptions, magnetic anomalies have the character and orientation consistent with the earth's field in its present orientation. This property is directly dependent on the susceptibilities of the rocks (equation 3.8); and consequently on the rocks' content of magnetic minerals (mainly magnetite).

On the other hand remanent magnetization is the part of rock magnetism retained from an earlier magnetization. In magnetic materials the relationship between the applied field intensity H and the resulting magnetization M in the mineral is more complicated than the simple proportionality given in equation 3.8. A more acurate relationship takes account of the magnetic 'history' of the material.

Suppose that the unmagnetized material, which is taken as magnetically isotropic, is placed in a zero field. The variation in its magnetization (M) with applied field (F) is shown in Fig. 3.2.

Remanent magnetization is often considered in the following groups:

1. Viscous Remanent Magnetization (VRM): When rocks remain in a magnetic field for a long time,

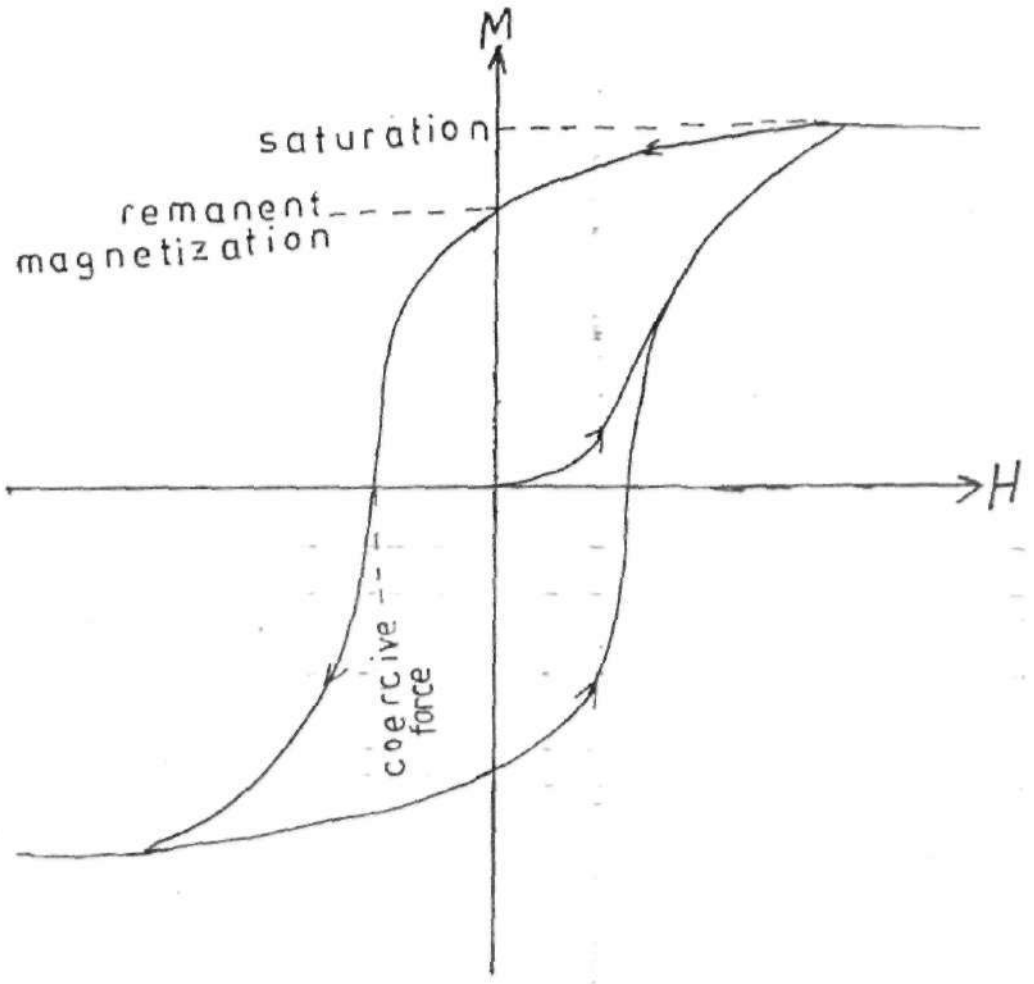


FIG 3.2

RELATION BETWEEN MAGNETIZATION(M) AND MAGNETIC FIELD INTENSITY FOR A MAGNETIC MINERAL.

some of their induced magnetism slowly becomes irreversible. This viscous magnetization generally increases as a logarithmic function of time. Thermally activated changes may also cause a slow loss of acquired magnetization (Parkinson, 1982).

2. Thermo-Remanent Magnetization (TRM): This is the most important mode of acquisition of remanent magnetization by igneous rocks. As the rocks solidify they cool through their curie points and a spontaneous magnetization develops when the magnetic grains in them get "frozen" in an alignment parallel to the surrounding magnetic field.

3. Chemical Remanent Magnetization (CRM): When a magnetic mineral forms, by chemical reaction, in a magnetic field it often acquires a remanence parallel to that field. This is often the case whenever ferromagnetic grains grow or are transformed from one form to another at a temperature below the curie point e.g. T_1-magnetite to maghemite (has more stable magnetization).

4. Detrital Remanent Magnetization (DRM): This is predominant in sub-aqueous sedimentary rocks. Some of the grains that settle at the bottom of the water are of magnetic minerals and they tend to be oriented by any magnetic field existing at the time of deposition. Thus when the rock is formed by

de-watering and consolidation of the sediments, the magnetic particles are mechanically held in a direction which reflects the direction of the field at the time of formation of the rock. Sub-aerial deposits of volcanic ash can also acquire remanent magnetization parallel to the ambient field (Steele, 1981).

5. Isothermal Renament Magnetization (IRM):
This is the magnetization acquired at low temperature by imposing and then removing a strong field, unlike in the case of TRM which is acquired by changing temperature in a weak field.

CHAPTER 4

DATA ANALYSIS (REDUCTION)

4.1 PRELIMINARY

The four aeromagnetic maps were digitized at 3km intervals. The field values so obtained were combined to make it continuous over the area. This combination gives a square grid of 37 x 37 grid points.

The following constants of the magnetic field over the area were established: the ambient magnetic field (Ho), the magnetic declination, and the magnetic inclination.

The magnetic field values over the area lie around an average value of 7825 nT. The total magnetic field value is obtained from this adding 25000nT.

$$Ho = 7825 + 25000 = 32,825nT$$

Magnetic declination over the area was obtained by interpolating from a world map of declination values (Parkinson, 1982), based on MAGSAT data (Langel et al, 1980). The declination was estimated to be about -5^{o} ($=355^{o}$ clockwise from North).

The aeromagnetic maps give inclination at the extreme south of Nigeria ($5^{o}N$) as 0^{o}, and inclination at extreme North ($13^{o}N$) as 9^{o}. By interpolation,

the magnetic inclination over the area of work was thus found to be : 5.25°.

From the magnetic field map of the area, the points presented on Table 4.1 could be noted concerning distinct anomalies. The predominance of negative anomalies indicates a greater abundance of the rock-types giving rise to them. Many of the positive anomalies are of much smaller magnitude than the negative anomalies.

There are some strong anomalies which cannot be correlated with any younger granite or basaltic rock-types. They overlie areas which have been mapped as basement rocks. These anomalies which are similar in characteristics to those correlated to younger Granite rock-types cannot be arising from basement rocks. Such anomalies can be reasonably deduced as arising from geological structures which are similar to the exposed Younger Granite complexes but which are buried beneath basement rocks. Seven such uncorrelated anomalies were found in the area of study. Their locations are given on Table 4.2 and illustrated on a geological map of the area (fig.4.1).

From Fig. 4.1 it can be seen that the location of anomaly No.1 if considered with the Koffia, Kwandonkaya, and Tongolo Younger Granite complexes, forms a linear trend in the NNW-SSE direction.

TABLE 4.1

PROPERTIES OF DISTINCT MAGNETIC

ANOMALIES IN AREA OF STUDY

PROPERTY	NUMBER OF ANOMALIES
ANOMALIES 15 nT	167
Positive Anomalies	69 (41.3%)
Negative Anomalies	98 (58.7%)
ANOMALIES 100 nT	7
Positive Anomalies	2
Negative Anomalies	5

Also, the locations of the anomalies No. 7, No. 3 and No.6 form another linear trend oriented in the same NNW-SSE direction. It can be noted that these trends are approximately parallel to the direction of elongation of the Sara-Fier complex. This can be interpreted as suggesting a common origin or mode of emplacement of the Sara-Fier and the buried Younger Granites. This may also be indicative of structural features in the basement complex; especially as it can be noted that the above trends are confined to those buried complexes east of the major Younger Granite massifs.

4.2 STATISTICAL ANALYSIS OF RESIDUAL FIELD AND GEOLOGICAL FEATURES

The method used in separating the residual and regional fields is the gridding method due to Griffin. At each grid point with field value M0 grid points M1, M2, M3, M4 are taken at one-grid spacing to the north, east, south and west of the point. The regional field value at the centre point is taken to be the mean of the values M1, M2, M3, M4.

$$\text{i.e. Regional field value} = \frac{M1+M2+M3+M4}{4}$$

$$\text{The residual field value} = M0 - \text{Regional field value}$$
$$= M0 - \tfrac{1}{4}(M1+M2+M3+M4).$$

The results were used in preparing contoured residual

TABLE 4.2

LOCATION OF ANOMALIES ARISING FROM

BURIED YOUNGER GRANITES

ANOMALY NUMBER	LATITUDE	LONGITUDE
1	9°50' - 9°58.33'	9°18.33' - 9°28.33
2	9°00' - 9°09'	8°30' - 8°39'
3	9°19' - 9°24'	9°15' - 9°21.67'
4	9°51.67' - 10°00'	8°30' - 8°37'
5	9°51.67' - 10°00'	8°37' - 8°42'
6	9°00' - 9°05.5'	9°24' - 9°30'
7	9°28.5' - 9°38.5'	9°08 - 9°17.5

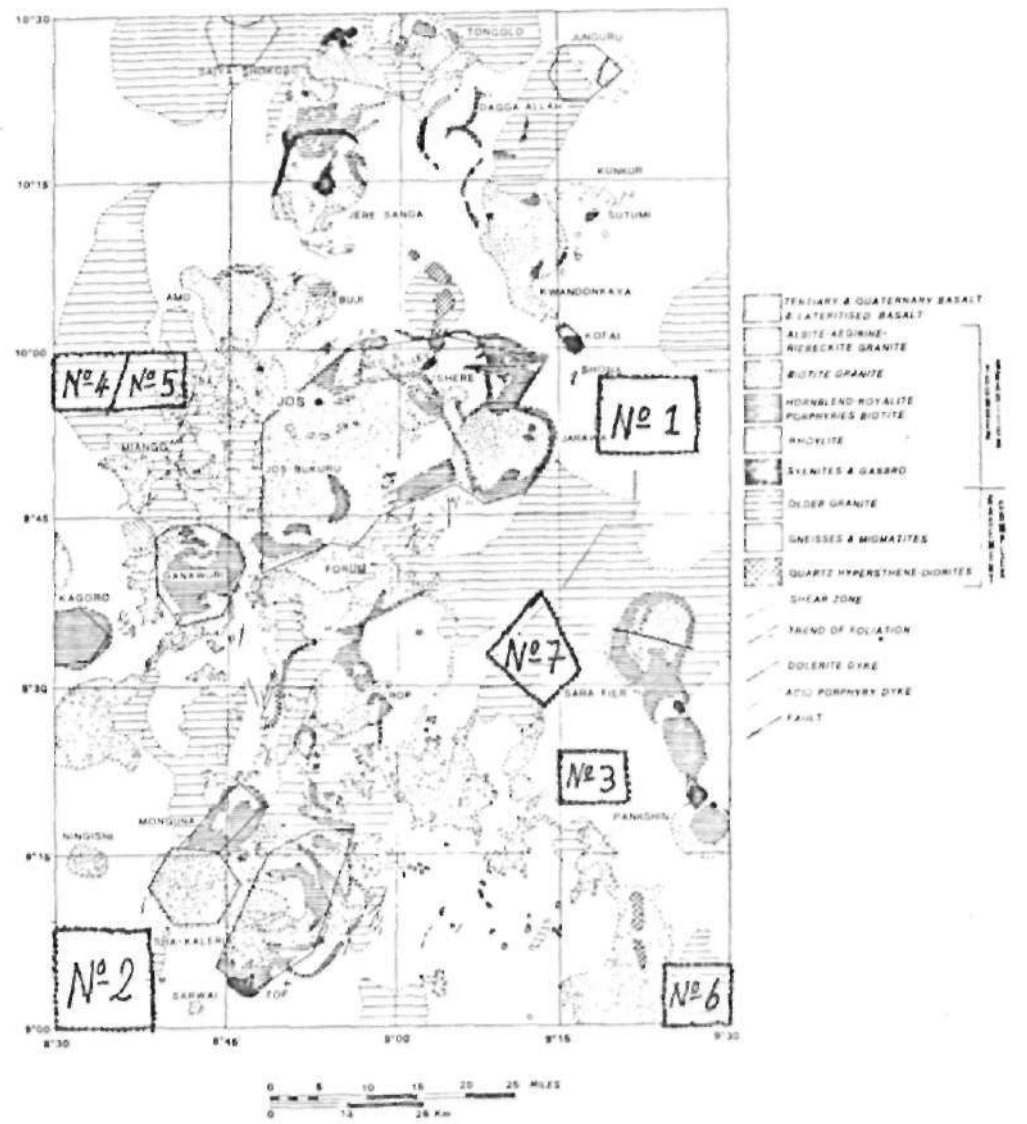


FIG 4.1

LOCATION OF ANOMALIES THOUGHT TO BE DUE TO BURIED YOUNGER GRANITES
(Adapted from Ajakaiye, 1982)

and regional maps of the area. By correlating the anomaly values and the rock-types over which they occur, the different magnetic signatures of the various rock-types were deduced.

The deductions were made from an elementary statistical analysis of the rock-types and their magnetic anomalies. The rock-types were divided into the following groups:

01 - Basalts

02 - Microgranites

03 - Riebeckite and Arfvedsonite Granites

04 - Biotite-Granites

05 - Hornblende-Granites

06 - Hornblende-Porphyries

07 - Rhyolites

08 - Basic rocks and syenites

09 - Basement rocks.

For each rocktype (i) the number of anomalies, (ii) the mean value of the anomaly fields (ii) the standard deviation for the anomaly field; were determined.

From the results (Table 4.3) those anomalies whose magnitudes and polarities are similar to those of the exposed Younger Granite rock-types but which have been located over areas mapped as basement rocks were suspected to be due to buried Younger Granites. From Table 4.3 it can also be seen that

negative field values are typical of acidic rock-types of the Younger Granite group. This indicates that they have a low content of ferromagnesian minerals.

4.3 MODELLING

4.3.1 INITIAL VALUE OF BODY PARAMETERS

Good initial values of the parameters of the bodies being modelled reduce the number of models to be tested, and hence the time required to arrive at a good fit. Initial values of susceptibility contrasts we deduced from Table 4.4. where the average susceptibility of acid igneous rocks is 650×10^{-6} emu and that of basic igneous rocks is 2600×10^{-6} emu, giving a mean volume of 1625×10^{-6} emu and that of basalt is 6000×10^{-6} emu. Thus initial contrast for granite was assumed to be -1425×10^{-6} emu and that for basalt as 4375×10^{-6} emu. These contrasts were used in modelling assuming the magnetization to be uniform throughout the modelled bodies.

For determining the initial depths to the tops of the anomalous bodies, the Half-slope depth estimation method developed by Peters (1949) was used. A profile is drawn through the anomaly so that maximum and minimum field valuesoccur along it (FIG.4.2).

TABLE 4.3

ELEMENTARY STATISTICAL QUANTITIES FOR THE ANOMALIES OCCURING OVER VARIOUS ROCKTYPES

ROCK-TYPES	NUMBER OF ANOMALIES	ANOMALY FIELD	
		MEAN VALUE (nT)	STANDARD DEVIATION(nT)
Basalts	45	+42.44	25.703
Microgranites	10	-35.30	29.507
Riebeckite and Arfvedsonite Granites	2	Anomalies too few	
Biotite - Granites	26	-38.81	37.995
Hornblende - Granites	33	-30.94	25.908
Hornblende-Porphyries	10	-37.00	34.670
Rhyolites	2	Anomalies too few	
Basic rocks	6	+62.50	45.729

TABIE 4.4

AVERAGE MAGNETIC SUSCEPTIBILITIES OF ROCKS OF THE YOUNGER GRANITE PROVINCE

ROCK TYPE	SUSCEPTIBILITY (emu)	*SUSCEPTIBILITY CONTRAST (emu)
Biotite Granite	0.00249381	-0.00238726
Granite Porphyry	0.002581667	-0.00299404
Riebeckite Granite	0.0073825	+0.002501425
Rhyolite	0.003274	-0.001606071
Micro Granite & Quartz Porphyry	0.003439	-0.001442071
Hornblende Biotite Granite & Hornblende Fayalite Granite	0.002772	-0.002109071
Crystalline Basement	0.004881071	0.0000
Average Younger Granite	0.00327166	-0.001607411

*Susceptibility contrast is with respect to the crystalline basement.

The half-slope parameter P is the horizontal distance between the points P_1 and P_2. The distance S is the slope parameter. The depth to the top of the body is approximately equal to S and also approximately equal to P/2 (Vacquier et al, 1951).

4.3.2. 3-DIMENSIONAL MAGNETIC MODELLING

The 3-dimensional magnetic modelling was carried out using a FORTRAN program based on the theory developed by Manik Talwani (1965). The essential aspect of this theory are presented in APPENDIX (1).

When the magnetization is taken as being by induction in the earth's field, the total intensity anomaly, T is given by

$$\triangle T = \triangle x \cos D \cos I + \triangle Y \sin D \cos I + \triangle z \sin I$$

where D is magnetic declination, I is the inclination of the field, and $\triangle x$, $\triangle Y$, $\triangle z$ are the three components of the anomaly magnetic field in the x, y, and z directions respectively.

The co-ordinates of the corners of the polygons which represent the contours on the model body, the co-ordinates of the points at which the magnetic anomaly is being determined and the values of k, Ho, I and D are fed into the computer, and the values of $\triangle x$, $\triangle y$, $\triangle z$ and $\triangle T$ are obtained. Only the total intensity ($\triangle T$) was required in this work.

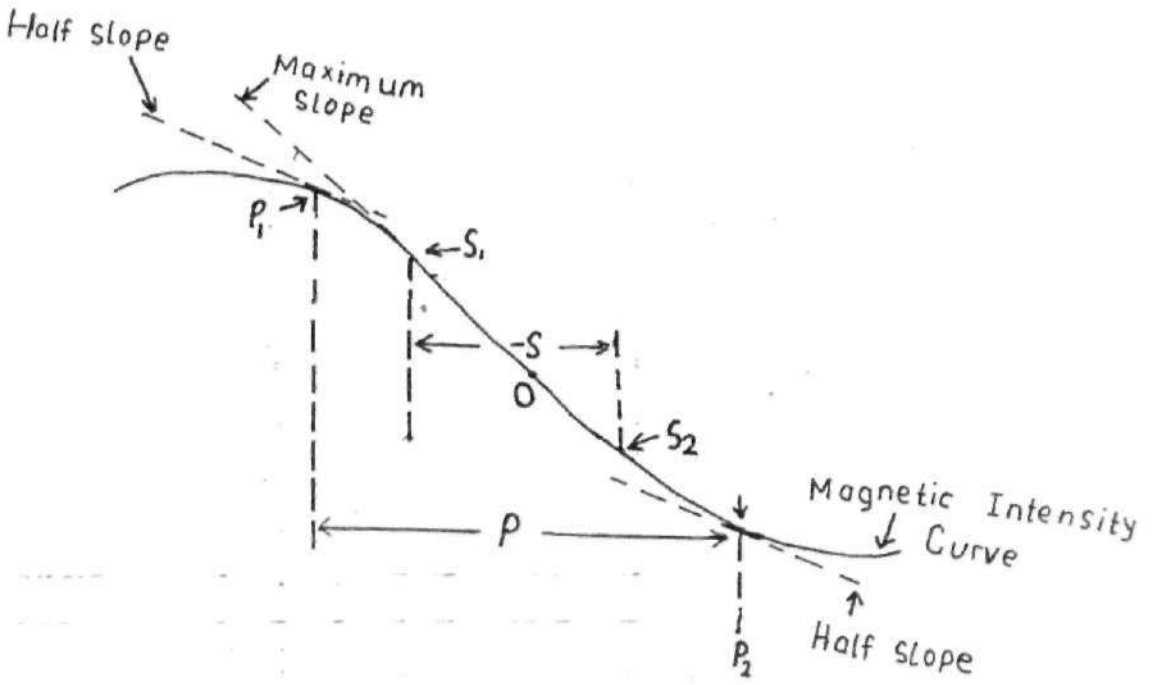


FIG 4·2

IDEALIZED MAGNETIC PROFILE FOR DEPTH ESTIMATION BY HALF-SLOPE METHOD

(From Nettleton, 1976)

The total intensity values generated from the model was compared with the measured anomaly values by a subroutine in the computer program which determined the correlation coefficient between the two sets of values. A model was considered good when the correlation coefficient was greater than 0.75. The susceptibility values were then adjusted to minimize the difference between the two sets of values.

CHAPTER 5

INTERPRETATION

The anomalies that were modelled are: No. 2, No. 3, No. 4 and No. 5. Anomaly No. 1 and Anomaly No. 7 consist, in effect, of groups of anomalies clustered together. Modelling of these was difficult because of the problem of resolution of the contribution from the different bodies. Anomaly No. 6 was not modelled because it is part of a much larger magnetic anomaly, a good part of which lies outside the area of study.

5.1 MODELLING OF ANOMALY NO. 2

The anomaly field is shown in fig. 5.1. The initial depth to the top is determined from the graph (Fig. 5.2) of the profile A-B. From the graph, initial depth to the top is determined (Table 5.1). Table 5.1 also shows the parameters of the bodies modelled for this anomaly.

The first body presents a susceptibility contrast (-0.001825 emu) which is common to Younger Granite rocks. The body lies fairly close to the surface. It has a highly irregular shape at depth (Fig. 5.3). This tends to indicate that there was some crustal movement after its implacement. Such crustal movement might have accompanied the erruption of the other bodies in its neighbourhood.

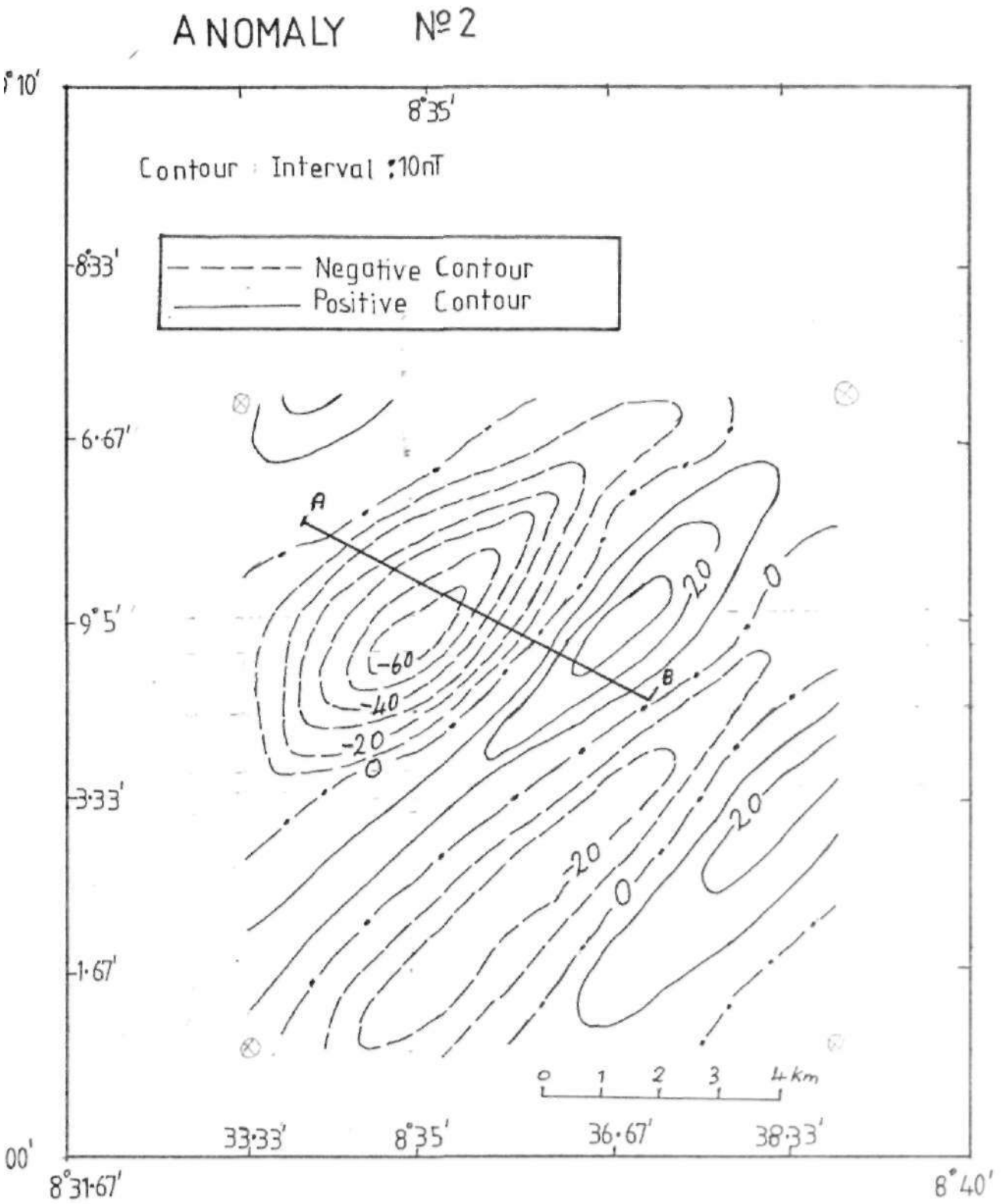


FIG 5·1
FIELD OF ANOMALY Nº2

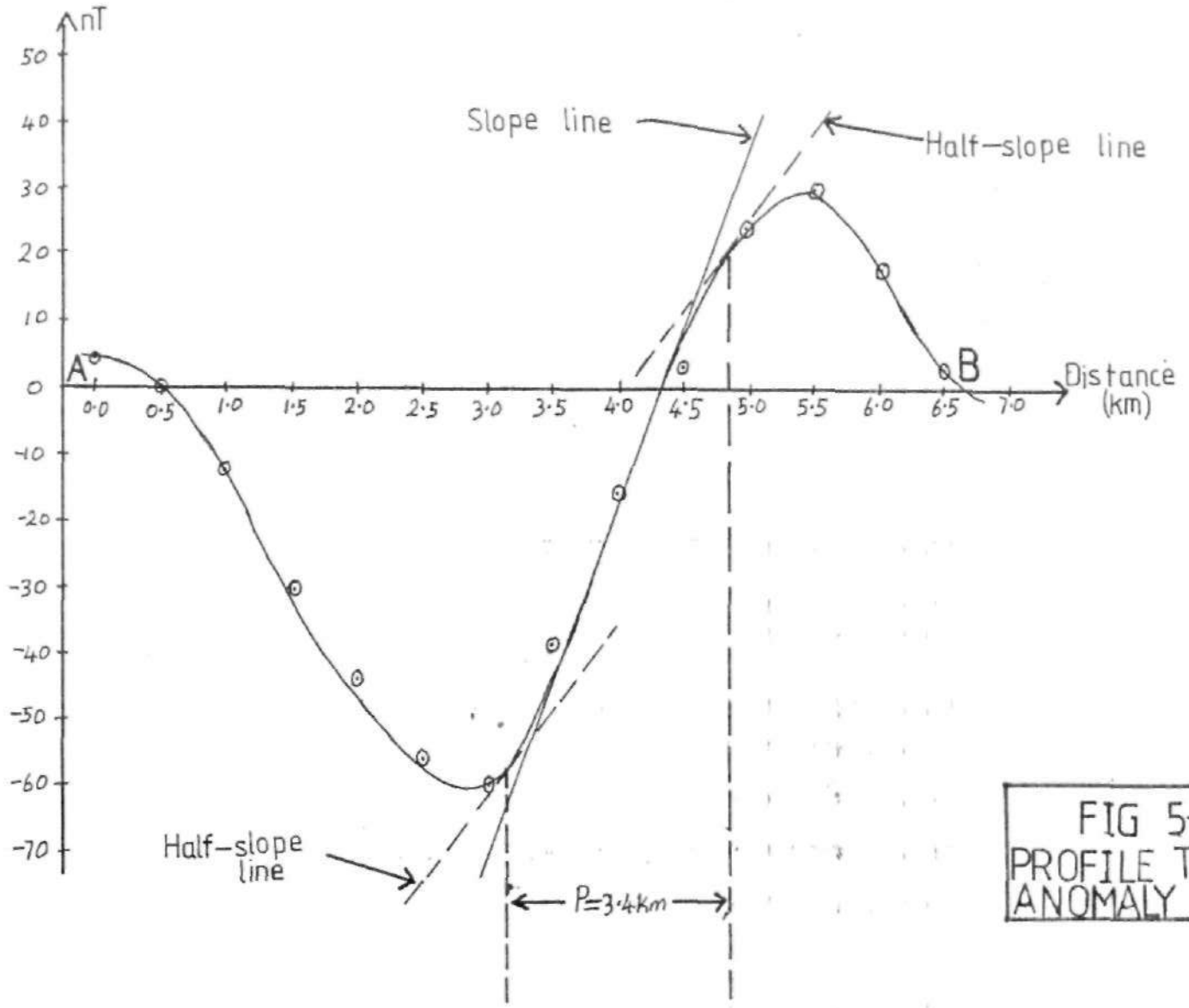


FIG 5-2
PROFILE THROUGH ANOMALY Nº2

The second body seems to be a basaltic intrusion. It is fairly tilted to the south at depth (Fig. 5.3). It is highly probable that its emplacement resulted in the deformation of the first body, and may have pushed it closer to the surface.

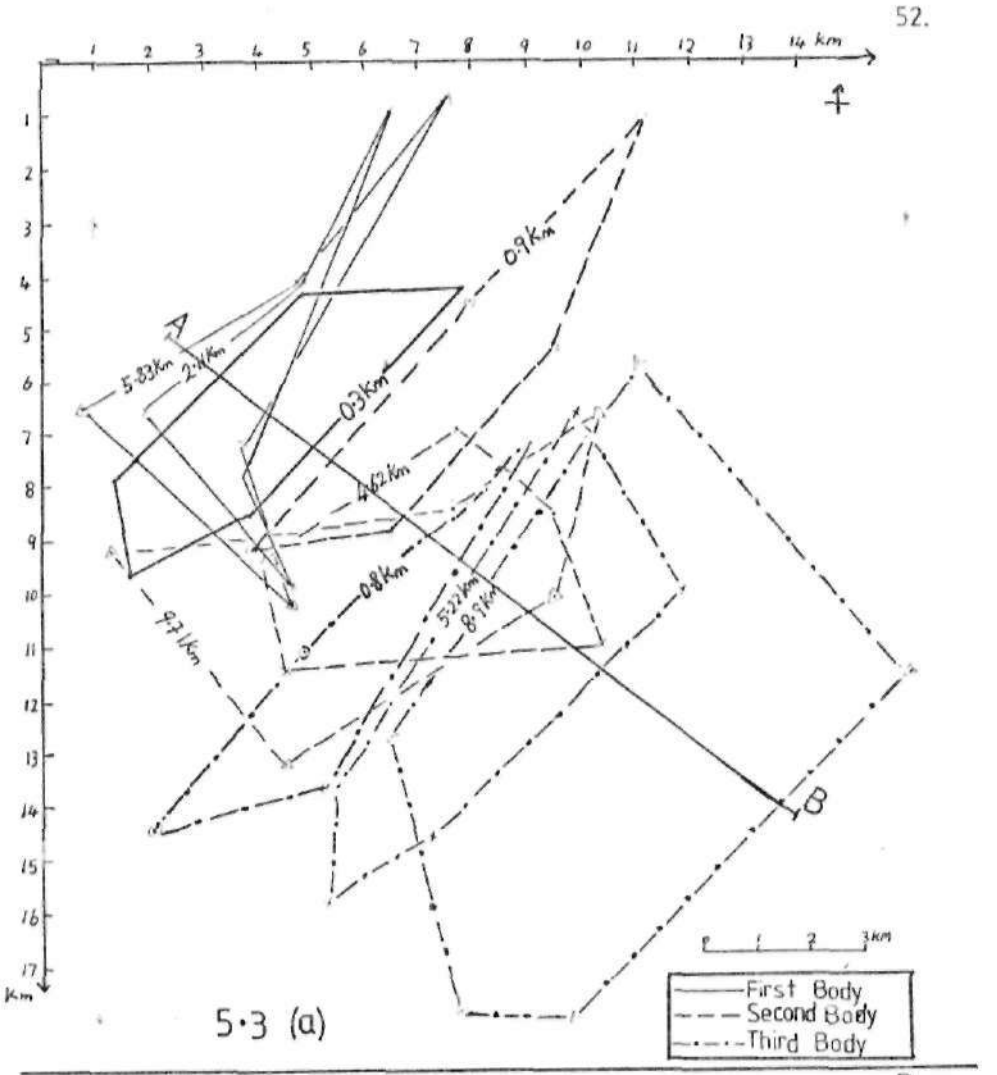
A third body is added because of the low negative field at the south-eastern part of the calculated field map. The resulting calculated field is shown in Fig. 5.4(c). The body is an elongated triangle at the top which becomes very wide towards its base (fig. 5.3). In addition to its low susceptibility contrast, it aopears that this body is a composite of a group of rock bodies (with higher susceptibility contrast) scattered in this area. A finer degree of modelling may resolve these bodies. It can also be seen that the second body cuts into this third one at depth. In addition to reinforcing the argument for a scattered group of rock intrusions, this latter fact indicate that the body (or group of bodies) was emplaced prior to the emplacement of the second body. Thus there was the emplacement of the Younger Granite rock-types (of negative susceptibility contrast) which was then followed by basaltic erruption between the areas occupied by the other rocks. It can be further observed that the first and third bodies are both shallower than the second, suggesting pressure forces from below.

TABLE 5.1

PARAMETERS OF MODELLED BODIES FOR ANOMALY NO.2

	First Body	Second Body	Third Body
Initial depth to top (km)	1.70	1.70	1.70
*Correlation Coefficient	0.51508	0.71717	0.8164
Susceptibility Contrast (emu)	-0.001825	+0.001025	-0.000775
Depth to the top (km)	0.3	0.9	0.8
Depth to the bottom (km)	5.83	9.71	8.90

*Maximum correlation coefficient between the calculated field and observed anomaly field addition of the body to the previous one(s).



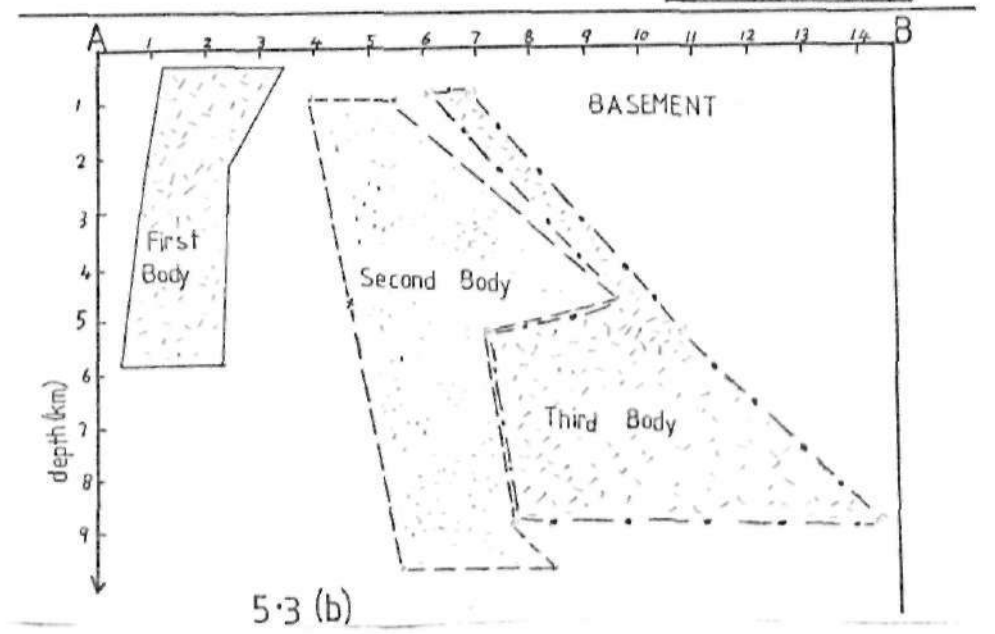
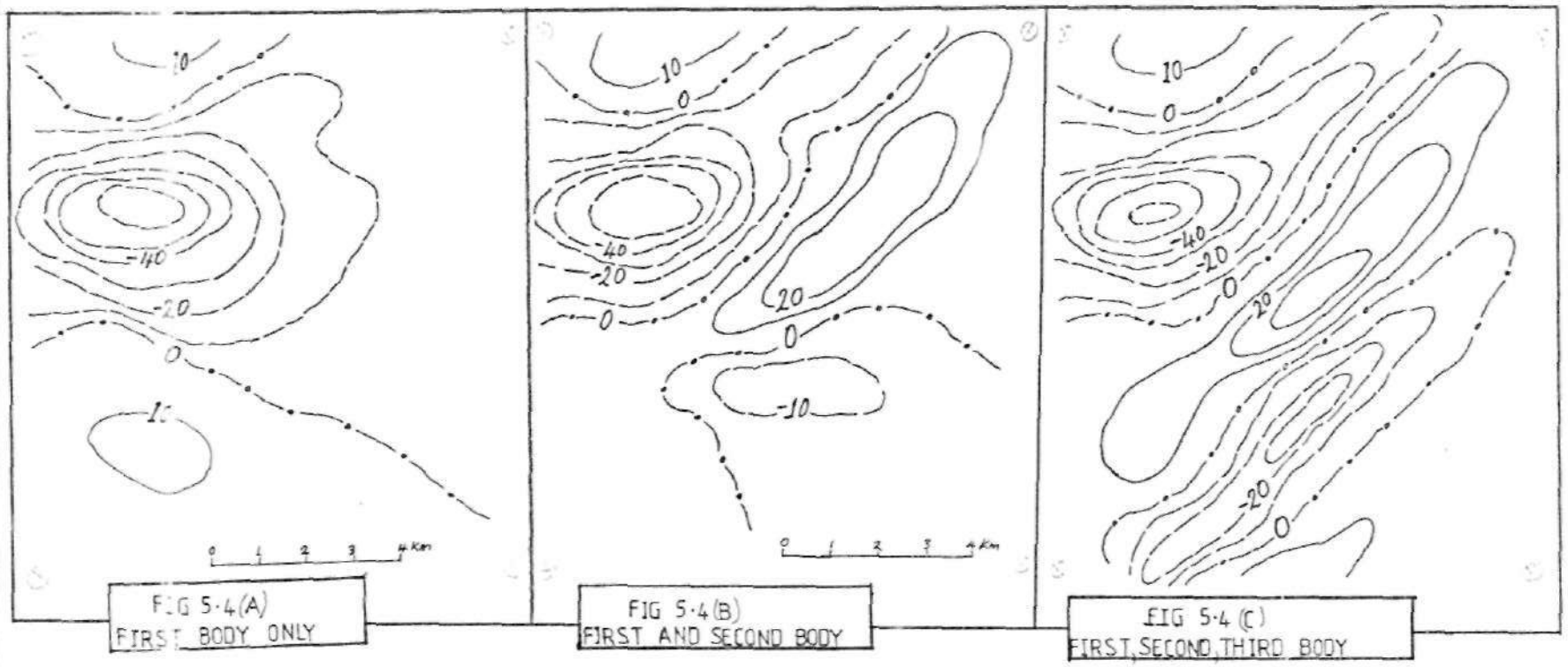


FIG 5·3
(a) MODELLED BODIES OF ANOMALY №2
(b) DEPTH PROFILE ACROSS THE BODIES



contour interval : 10nT

FIG 5·4
CALCULATED FIELDS FOR ANOMALY Nº2

5.2 MODELLING OF ANOMALY NO. 3

The anomaly is shown in fig. 5.5. The graph in Fig. 5.6 is a plot of the profile A-B across the anomaly for determining the initial depth to the top of the body (Table 5.2). Table 5.2 also shows the parameters of the bodies modelled for this anomaly. Fig. 5.7 shows the calculated fields after the addition of successive bodies.

The outline of the modelled bodies is shown in Fig. 5.8. It can be seen from the figure that the first body is approximately rectangular at the top and broadens out to a large triangle at base. It can also be noted that the body tilts southwards towards the base. The middle and the bottom contours have a pronounced narrow eastward extension which may be due to an easterly extending joint in the basement that was filled by the intruding magma. The susceptibility contrast (-0.001825 emu) lies within the range of values for Younger Granite rock-types.

It can be seen from Fig. 5.7 (A) that the positive field lying to the north of the dominant negative closure is of a much smaller magnitude than that in the observed anomaly (Fig. 5.5). Hence a second body of positive susceptibility contrast was added to the north of the first body. The "best" field obtained upon addition of the second body is shown in Fig. 5.7(B).

291940

291941

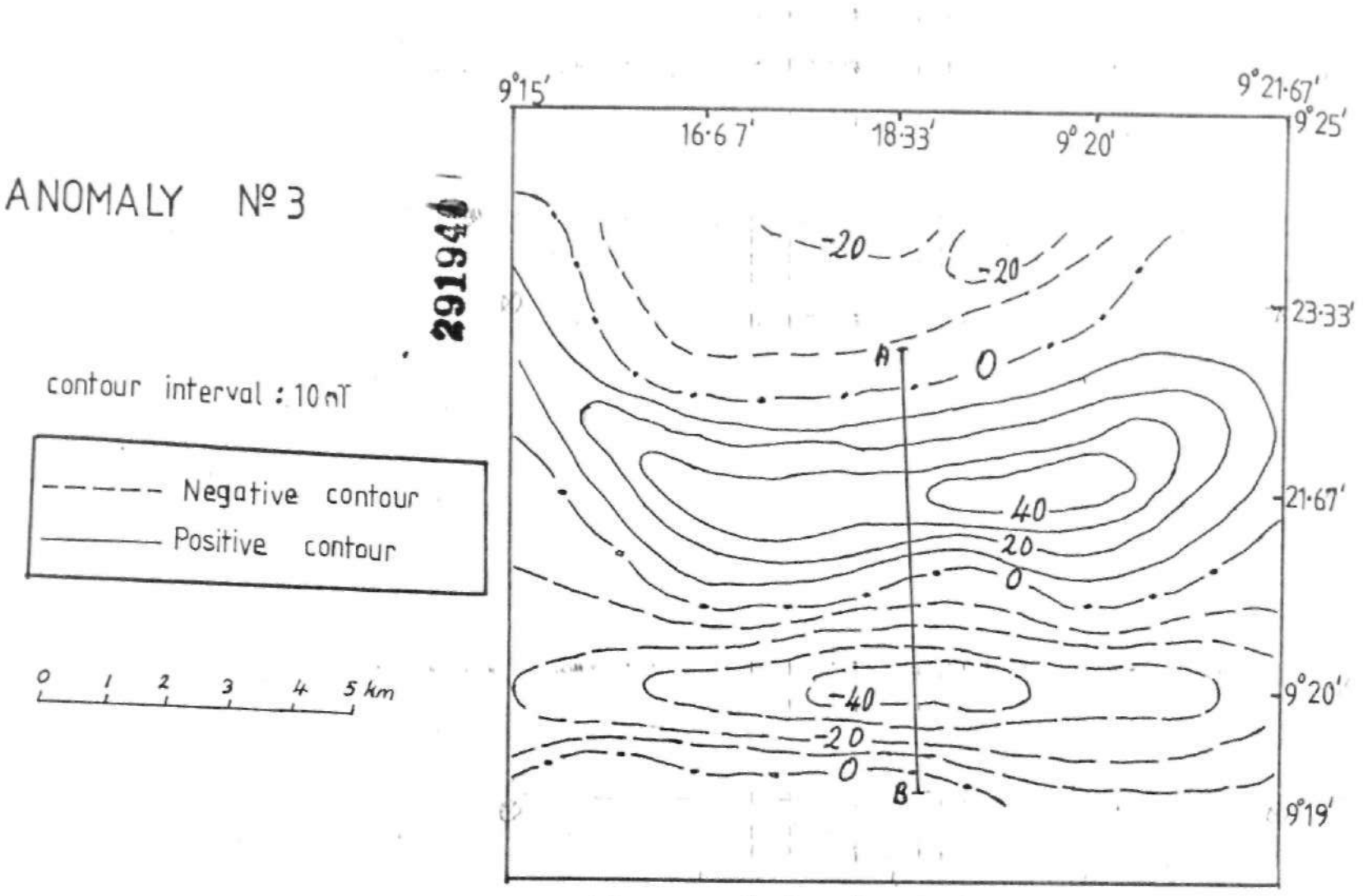


FIG 5·5
FIELD OF ANOMALY Nº3

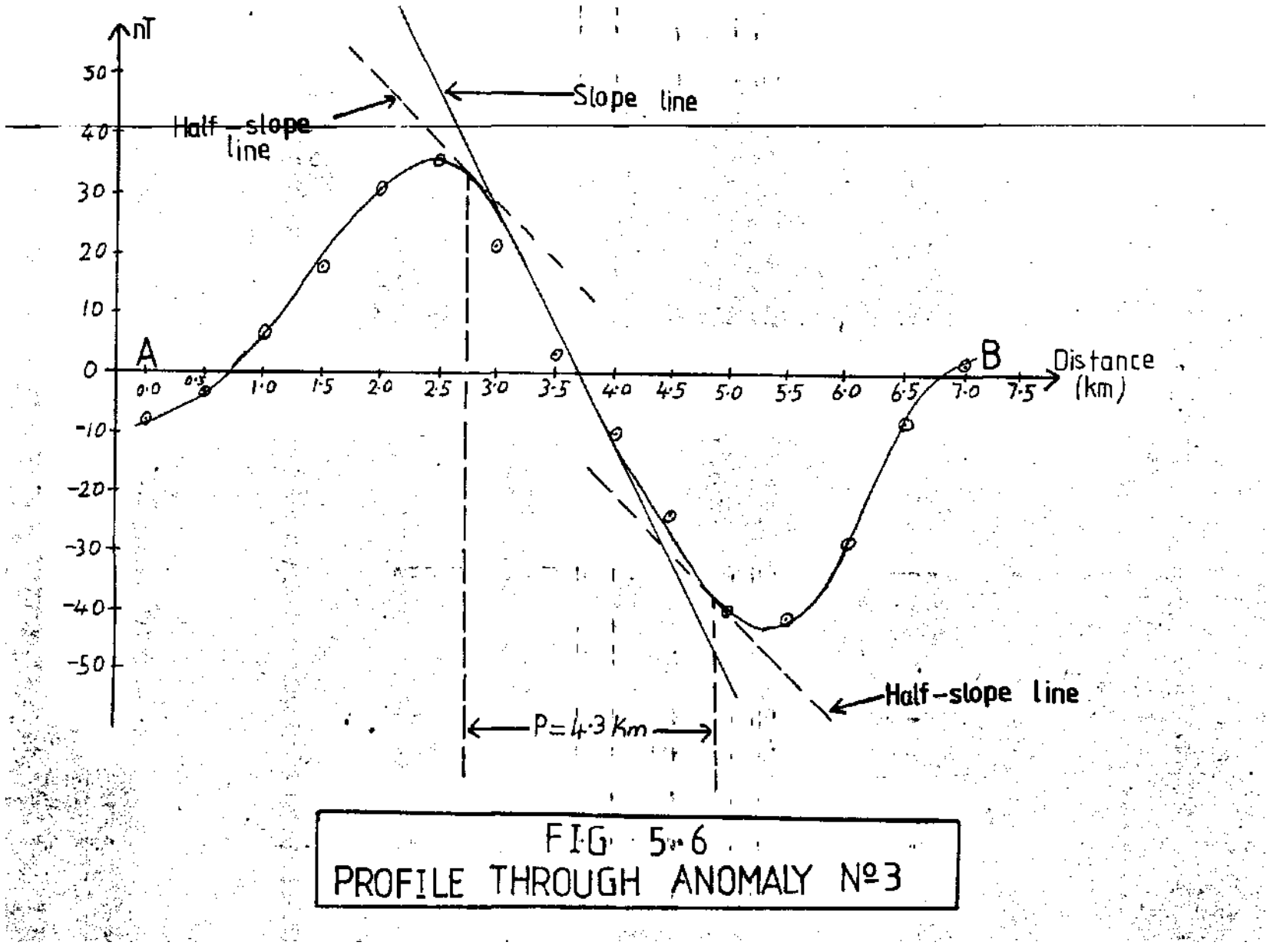


FIG 5.6
PROFILE THROUGH ANOMALY Nº3

TABLE 5.2

PARAMETERS OF MODELLED BODIES FOR ANOMALY NO. 3

	First Body	Second Body
Initial depth to top (km)	2.15	2.15
*Correlation Co-efficient	0.84093	0.93208
Susceptibility Contrast (emu)	-0.001825	+0.000825
Depth to the top (km)	1.95	1.20
Depth to bottom (km)	8.24	4.62

*Maximum correlation co-efficient between the calculated field and observed anomaly field after addition of the body to the previous one(s).

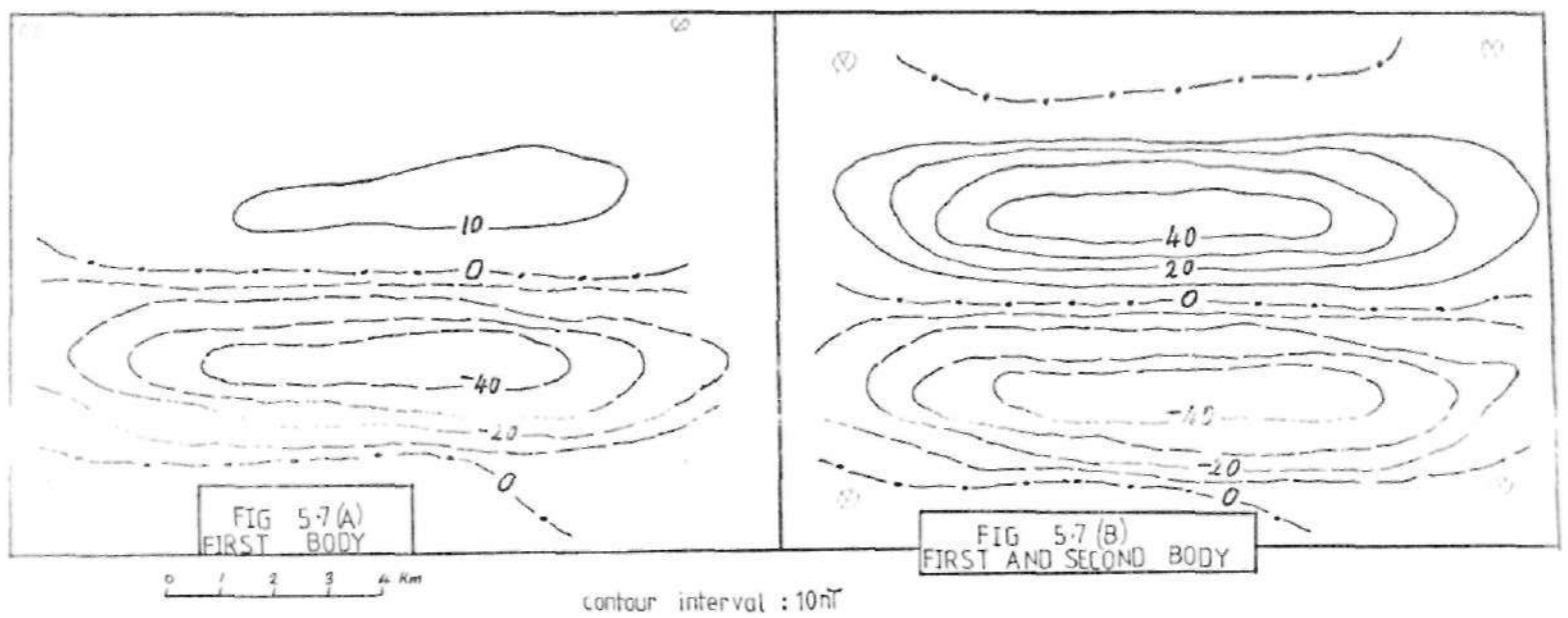


FIG 5·7
CALCULATED FIELDS FOR ANOMALY Nº3

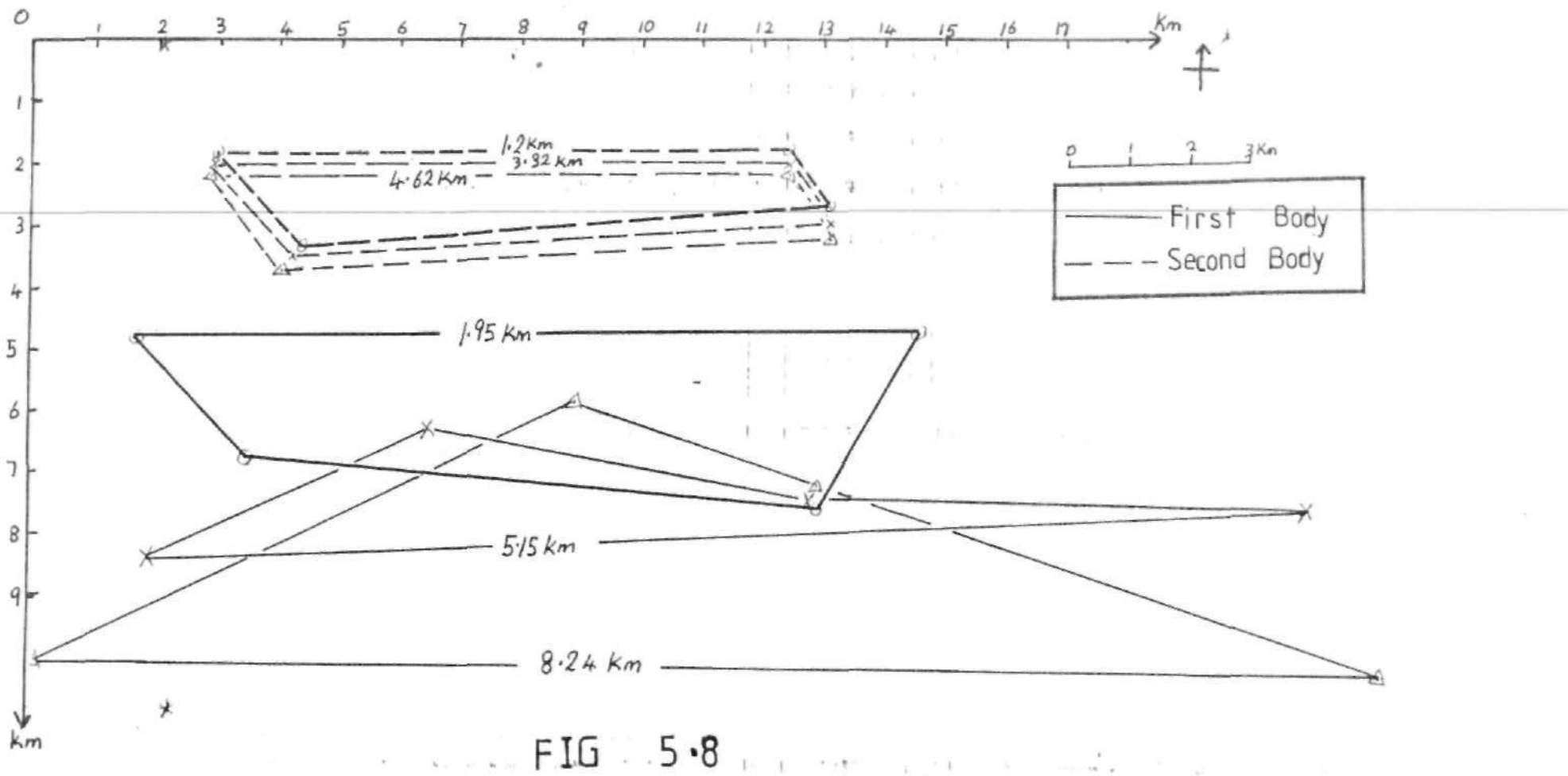


FIG 5.8

MODELLED BODIES OF ANOMALY Nº 3

The geometric form of the body (Fig. 5.8) shows it as a vertical structure with a near rectangular cross-section. It also has a moderate depth extent. These facts together with the susceptibility contrast (-0.000825) tend to indicate that this body is a basic rock, which as stated in chapter 2, can be commonly found around the margins of many Younger Granite massifs.

5.3 MODELLING ANOMALY NO. 4

The contoured field of this anomaly is shown on Fig. 5.9. The profile A-B is taken to determine initial depth to the top of the body. A plot of this profile is shown in Fig. 5.10. The initial depth to the top and parameters of the modelled bodies for this anomaly are presented on Table 5.3.

Assuming that the anomaly is due to a single body, the calculated field having highest correlation with the observed field is shown on Fig. 5.11(A). The geometric outline of this body is shown on Fig. 5.12. The body is smaller at depth and widens up towards the top, developing a prominent branch towards the north-east. This extension may be due to a fissure in the basement complex. One can also note the relatively moderate depth extent and the highly negative susceptibility contrast (-0.00425 emu). This latter point

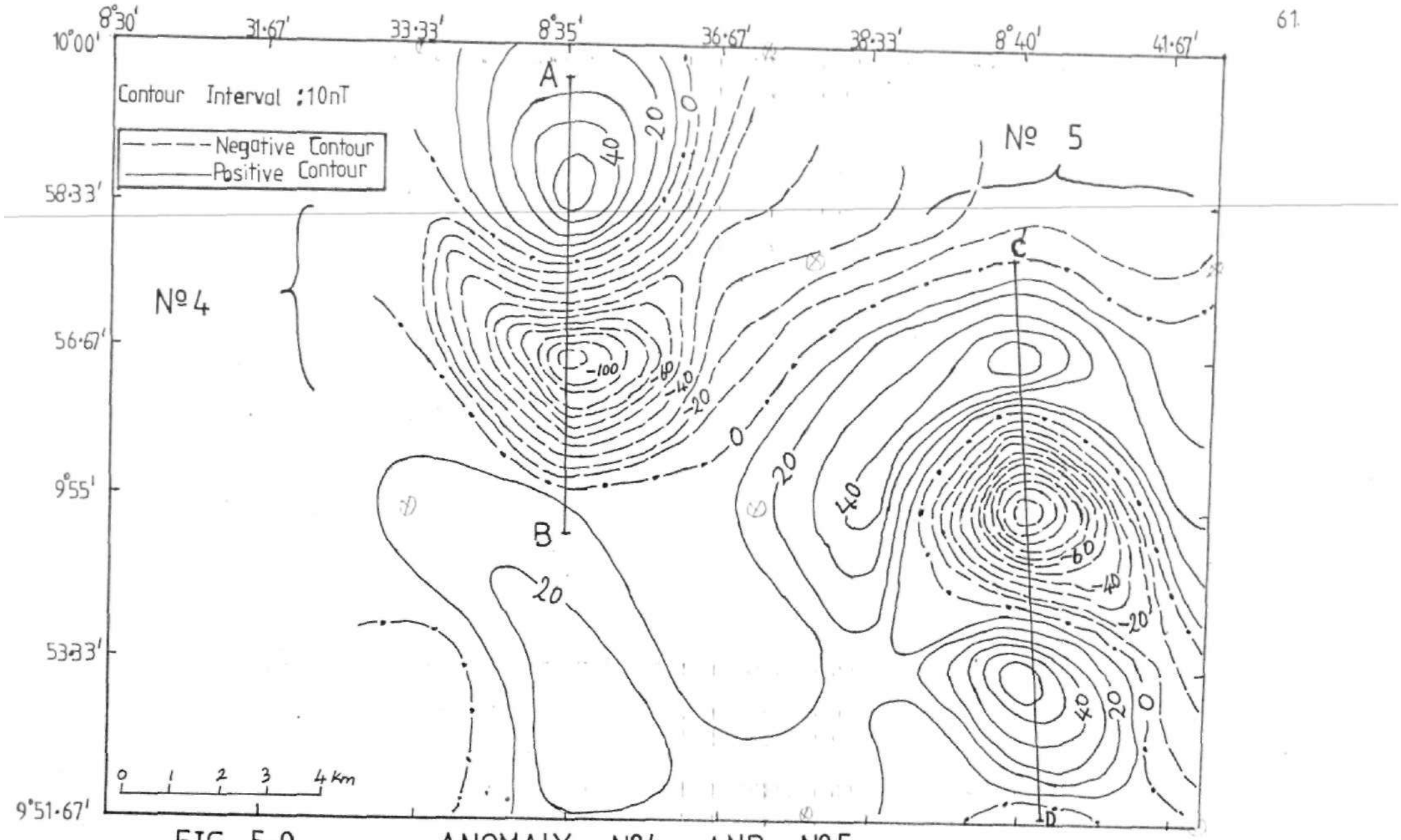


FIG 5·9 ANOMALY №4 AND №5

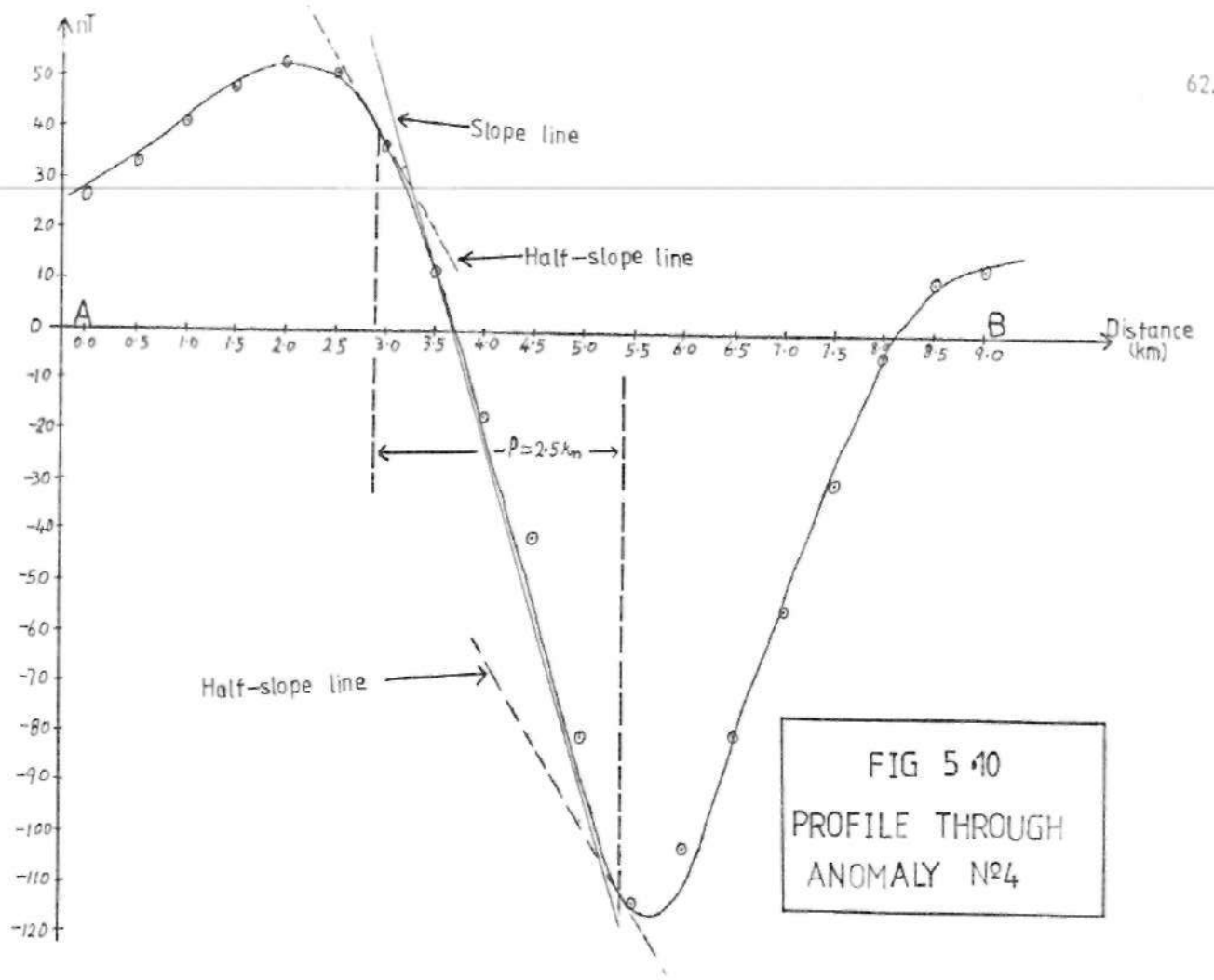


FIG 5·10
PROFILE THROUGH
ANOMALY Nº4

TABLE 5.3

PARAMETERS OF MODELLED BODIES FOR ANOMALY NO. 4

	First Body	Second Body
Initial depth to top (km)	1.25	1.25
*Correlation Coefficient	0.84045	0.87165
Susceptibility Contrast (emu)	-0.00425	+0.000625
Depth to the top (km)	1.45	0.85
Depth to bottom (km)	3.10	7.30

*Maximum correlation coefficient between the calculated field and observed anomaly field after addition of the body to the previous one(s).

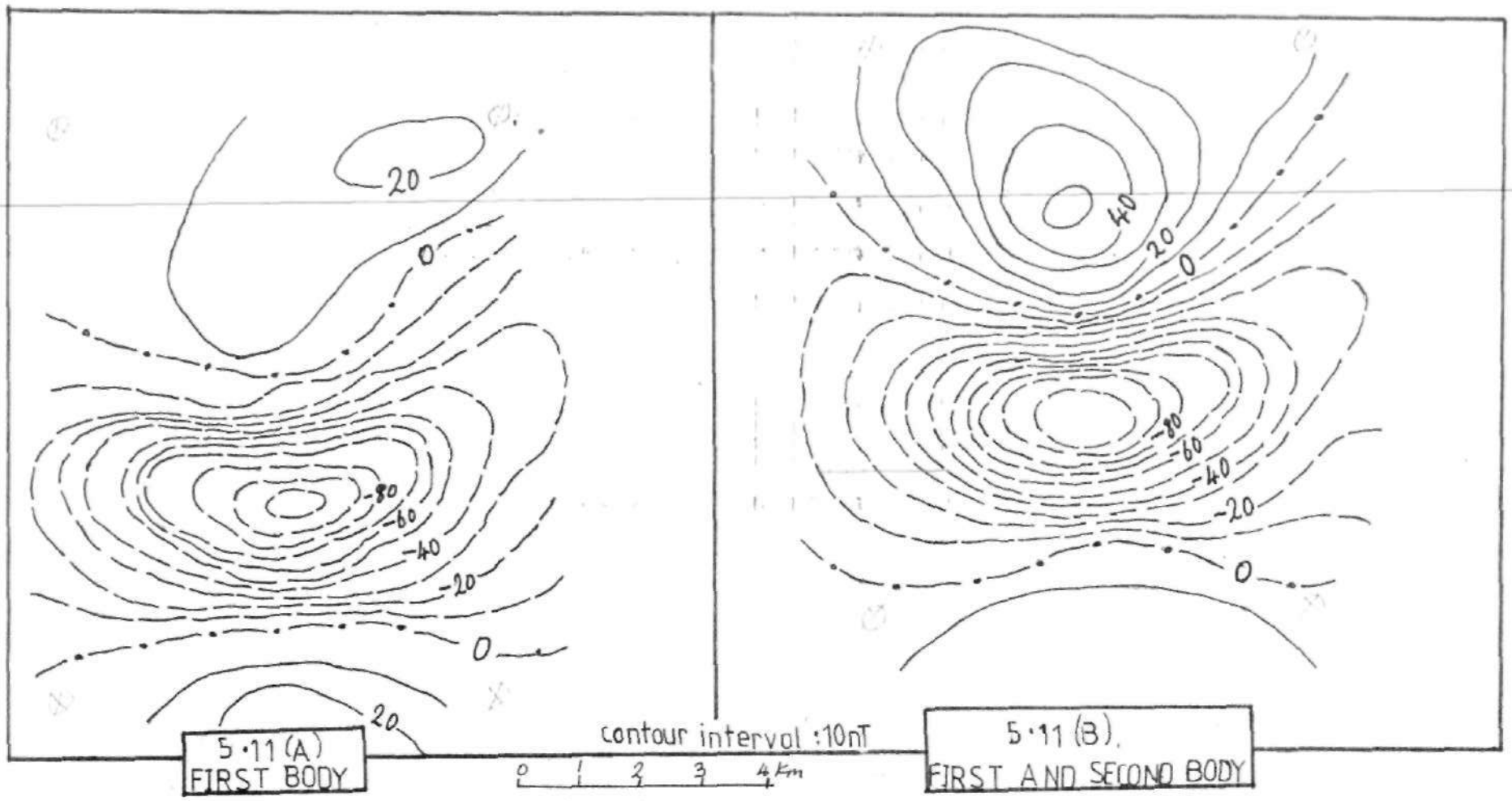


FIG 5·11
CALCULATED FIELDS FOR ANOMALY №4

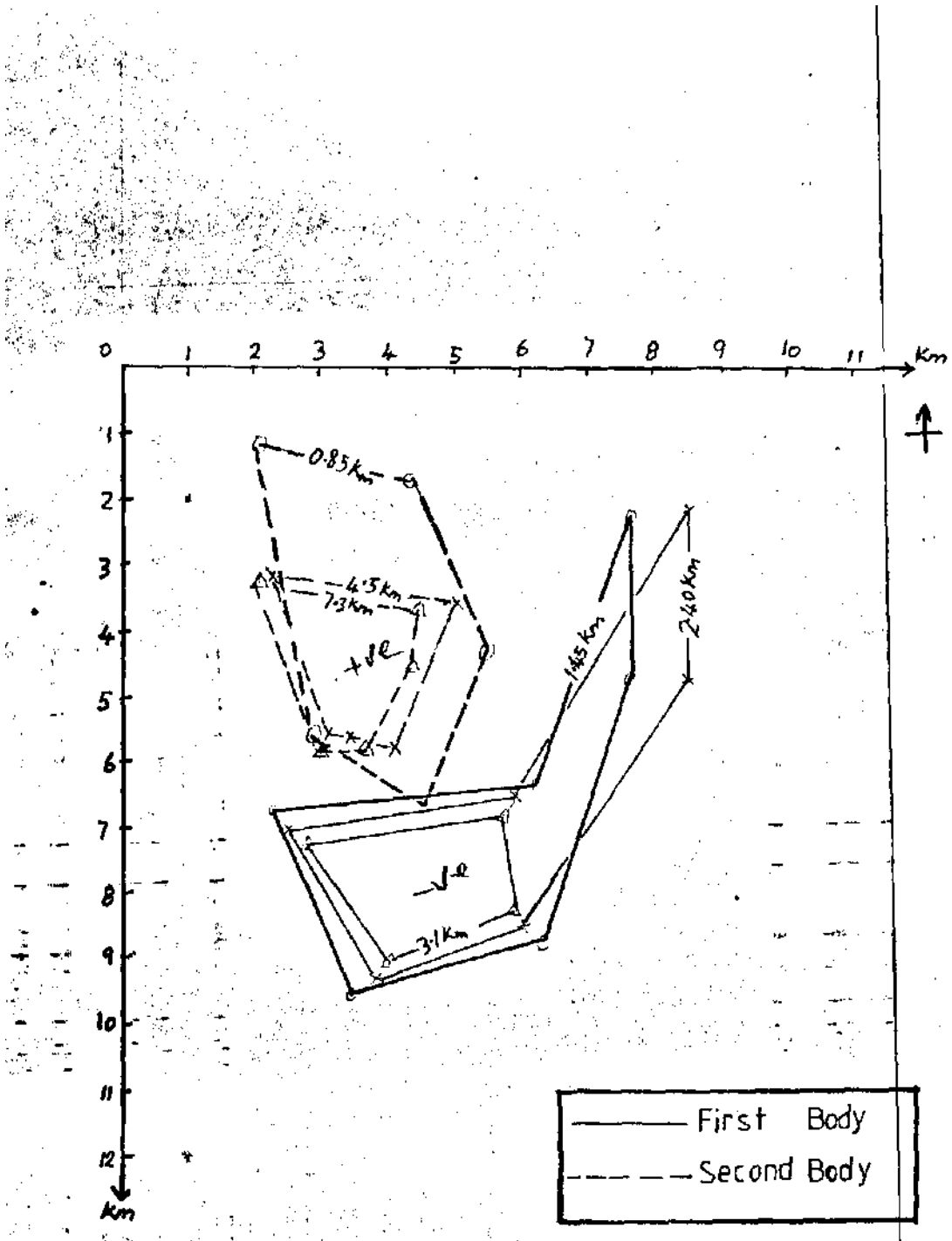


FIG 5.12

MODELLED BODIES FOR ANOMALY Nº4

strongly suggests that the composition of the body is of the acidic Younger Granite rocks. The geometry of the body takes on the curved outline common to many Younger Granite Complexes.

It can be seen from a comparison of fig. 5.11(A) with the observed anomaly (fig. 5.9) that the positive field to the north of 5.11(A) is much smaller than that in the observed anomaly. This suggests that another body of positive susceptibility contrast exists to the north of the body. When a second body was inserted in the model the combined calculated field with highest correlation (0.87165) with the observed field is shown in fig. 5.11(B). The body spreads out to cover a much wider area at a depth of 0.85km than it does at lower depths. The positive susceptibility contrast (+0.000625 emu) suggests that the body may be a basic plug possibly made up of basaltic or other rocks (dolerite, diorites, etc).

5.4 MODELLING ANOMALY NO. 5

This anomaly is to the east of anomaly No. 4 on fig. 5.9. The profile C-D was taken to determine the initial depth to the top of the body. The plot on Fig. 5.13 yields the initial depth to the top. This is presented on Table 5.4 together with parameters of modelled bodies for this anomaly.

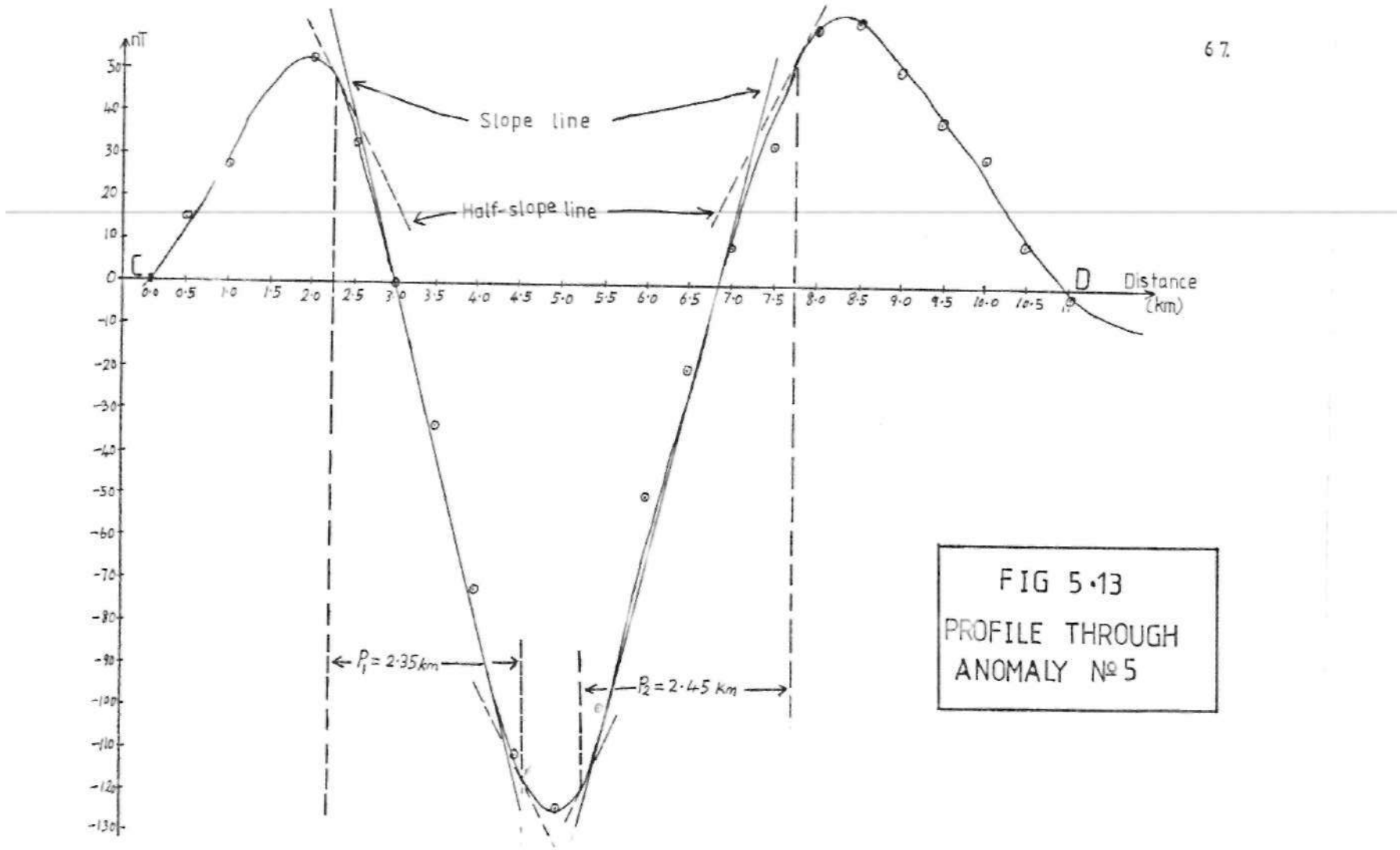


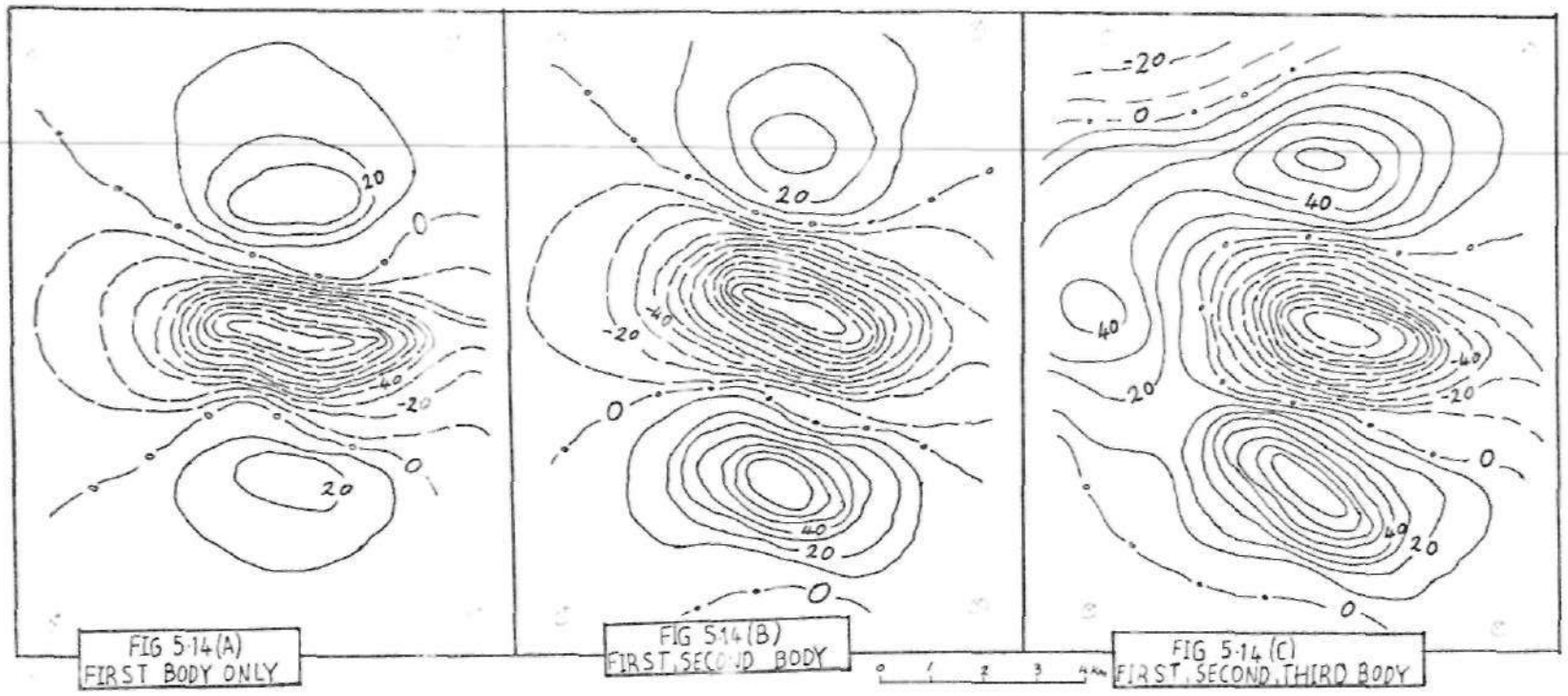
FIG 5·13
PROFILE THROUGH ANOMALY Nº 5

TABLE 5.4

PARAMETERS OF MODELLED BODIES FOR ANOMALY NO. 5

	First Body	Second Body	Third Body
Initial depth to top (km)	1.20	1.20	1.20
*Correlation Coefficient	0.66628	0.75181	0.86872
Susceptibility Contrast (emu)	-0.003775	+0.001525	+0.00150
Depth to the top (km)	1.62	1.02	1.32
Depth to bottom (km)	14.24	10.70	6.90

*Maximum correlation co-efficient between the calculated field and observed anomaly field after addition of the body to the previous one(s).



Contour interval : 10nT

FIG 5·14
CALCULATED FIELDS FOR ANOMALY Nº5

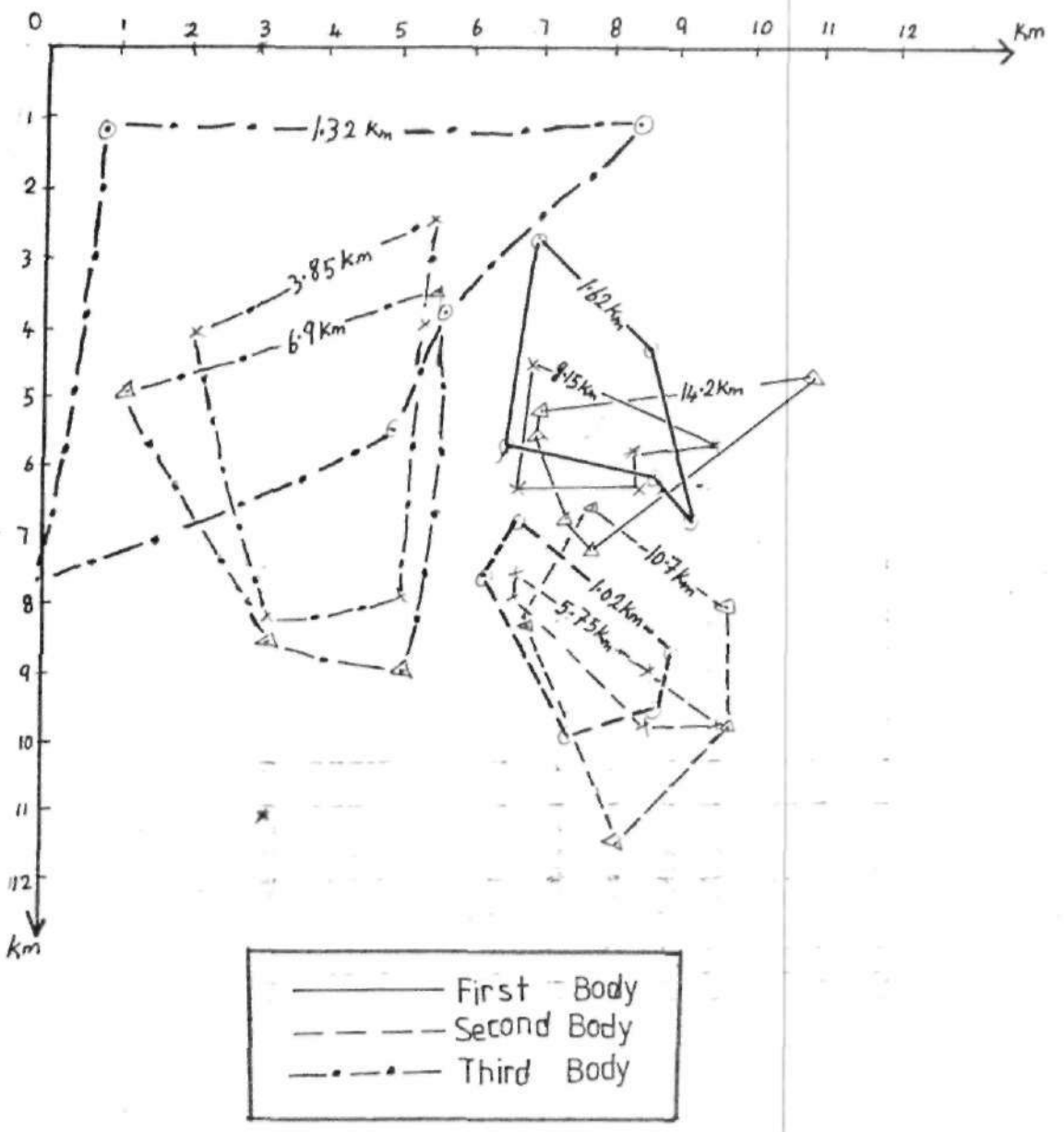


FIG 5·15

MODELLED BODIES OF ANOMALY Nº5

Modelling for one body, the best correlation co-efficient (0.66628) with the observed field is obtained for the calculated field shown in Fig. 5.14(A). The body (Fig.5.15) has the geometric form of a plug whose bottom outline is only a rotated form of the outline at the top. The susceptibility contrast (-0.003775 emu). The small correlation coefficient indicates that the one-body model is inadequate.

The addition of the second body yields the calculated fields shown in fig. 5.14 (B). The geometric outline of the modelled body (Fig.5.13) is in the form of two cones whose apexes meet at the middle contour.

Even after the addition of the second body the calculated field presents significant differences with observed field especially to the north-western part of the anomaly. Hence a third body was added to the model. The resulting field is shown in Fig. 5.14 (C).

5.5 DEDUCTIONS FROM THE MODELS

The models obtained have shown that the buried Younger Granites are near-vertical structures with polygonal cross-sections. The polygonal cross-sections agree with the type of fractures in the basement that would result from persistent upward

pressure by an underlying magma, giving rise to the subsidence of the roof-rocks and displacement of part of the magma towards the surface (MacLeod and Turner, 1965).

The susceptibility contrasts (-0.00183 emu, -0.00078 emu, -0.00425 emu, -0.00375 emu, +0.000625 emu, +0.000825 emu, +0.00103 emu, +0.00150 emu, +0.00152 emu) obtained for the modelled bodies are of the same order of magnitude as those obtained during isolated determinations carried out among the exposed Younger Granite Complexes from August to October, of 1983 (Table 4.4).

Furthermore, the depths of the structures obtained are:

depth to top : 0.3km, 0.8km, 0.9km, 1.0km, 1.2km, 1.3km, 1.5km, 1.6km, 2.0km.

depths to bottom: 3.1km, 4.6km, 5.8km, 6.9km, 7.3km, 8.2km, 8.9km, 9.7km, 10.7km, 14.2km.

These depth values are similar to those obtained for the modelling of the exposed Younger Granite massifs (2km to 12km).

CHAPTER 6

CONCLUSION

6.1 SUMMARY AND DISCUSSIONS

In the modelling carried out in this work, it has been assumed that the magnetic field arising from the structures is induced, and that the remanent part is negligible. It is probable that remanent magnetization in the Younger Granites may be significant. The remanence is likely to arise from viscous remanent magnetization (VRM). Being an upland area, there is likely to be some contribution from isothermal remanent magnetization (IRM) accompanying lightning strokes. Apart from this neglect of remanent magnetization, limitations in the models are introduced by two factors: Geometrically the number of contours for each body (3) and the number of points on each contour (5) cannot give an accurate outline of the bodies except for simple shapes e.g. prisms. Also susceptibility is not likely to be the same over each body as has been assumed for uniform magnetization of the bodies.

The conclusions that can be drawn from the work presented in this thesis are as follows:

1. From the residual anomaly maps of the area, a clear correlation can be made between negative magnetic anomalies and acidic Younger Granite rock bodies. This is consistent with the findings of earlier works on this area. This correlation leads to the supposition that similar magnetic anomalies lying over basement rock-types are due to Younger Granites burried below the surface.

2. The negative susceptibility obtained for the modelled bodies (-0.00183emu, -0.00078emu, -0.00425 emu, -0.00375 emu) are close to the average values that have been obtained by recent isolated susceptibility determinations among the exposed Younger Granite complexes (Younger Granite: -0.0016 emu, Biotite Granite: -0.0024 emu).

3. The models obtained have shown that the buried Younger Granites are near-vertical structures of polygonal cross-section. This is consistent with the shapes obtained by Ajakaiye et al, (1982) after modelling many of the exposed Younger Granite masses. The polygonal cross-sections agree with the type of fractures in the basement that would result from persistent upward pressure by the underlying magma, giving rise to doming distension of roof rocks under temsional conditions.

4. The depths obtained for the burried structures: 0.3 - 5.8km, 0.9 - 9.7km, 0.8 - 8.9km, 2.0 - 8.2km, 1.2 - 4.6km, 1.5 - 3.1km, 0.9 - 7.3km, 1.6 - 14.2km, 1.0 - 10.7km, 1.3 - 6.9km, agree with the range of values 2 - 12km obtained by Ajakaiye et al, from modelling of exposed complexes.

5. The existence of these buried Younger Granites fits in very well with the theory proposed by Turner (1974) concerning the structural and petrological evolution of the Nigerian Ring complexes. He postulated that the final stage in the evolution could be considered as a waning phase of igneous activity in which successively smaller granite intrusions were emplaced at increasingly deeper levels (such as those at which buried complexes occur). He correlated this with cooling conditions in the magma reservoir.

6. The existence of strong positive magnetic anomalies close to the negative anomalies arising from the buried Younger Granite rocks has been interpreted here as being due to basalts and basic rocks. The occurence of basaltic eruptions close to Younger Granite intrusions can be explained by the fact that the areas occupied by the granites already constituted fractures in the basement complex, and thus zones of weakness favourable for basaltic outflows.

It has been observed in the vicinity of the exposed Younger Granites that basic rocks, in the form of dolerites and basalts occur as lava flows, dykes and semi-concordant intrusions in the rhyolites and granites of many of the complexes. Also around the margins of the Younger Granite massifs it is common to find swarms of basic dykes (Turner and MacLeod, 1971). It is then not surprising that similar rock-types should occur around the buried complexes. The rocks giving rise to the positive field values could be divided into two groups: those having high positive susceptibility contrasts (+0.00152 emu for anomaly No. 5, +0.00103 emu for anomaly No.2) are probably basalts, while those with low positive susceptibility contrasts (+0.000625 emu for anomaly No. 4, +0.000825 emu for anomaly No. 3) are basic/ultra basic rocks such as gabbros, diorites and dolerites.

7. The modelled bodies also indicate that many of the bodies with negative susceptibility contrast show a more irregular shape than those with positive susceptibility contrast. This can be explained by assuming that the former bodies (possibly the acidic phase of the Younger Granites) have been deformed after their emplacement. Such deformation would have been brought about by a mechanism involving crustal

instability assuming that the eruption of the basalts, which took place after the emplacement of the Younger Granites, was accompanied by crustal movements. In the model of Anomaly No. 2, it can be seen that the basaltic body cuts into the Younger Granite rocks. This shows that chronologically the basalt is the younger of the two intrusions. This same order has also been widely accepted as the sequence of eruption of the exposed Younger Granites and Basalts (McLeod, 1971).

8. This work also shows evidence of a NNW-SSE trend in the location of some of the exposed and buried Younger Granite complexes in the area investigated. The fact that this trend exists only for complexes lying to the east of the large massifs (Jos-Bukuru-Sha-Kaleri) emphasizes the concept of basement control in the emplacement of the Younger Granites. Structural trends in the basement to the west of the central Plateau are north-south while to the east, north-north-west alignments have been found parallel to the zones of shearing in the basement (MacLeod et al, 1971).

6.2 SUGGESTIONS FOR FURTHER WORK

As noted above, remanent magnetization has been neglected in computation of the models. In view of

the serious modifications that remanent magnetization can make to the above results, it is necessary to determine the remanent magnetization in the Younger Granites rocks.

Apart from direct measurements in the laboratory on samples collected, an indirect method of determining remanent magnetization is also possible. The indirect method should be particularly useful in the case of buried Younger Granites whose samples may be more difficult to obtain. One such method is suggested by Shurbet, Keller and Friess (1976) in which remanent magnetization in geologic structures can be determined by a comparison of the gravity and magnetic anomalies arising from the bodies. Detailed gravity surveys would first be carried out over the buried Younger Granites. This would then be followed by three-dimensional modelling of the gravity anomaly obtained. Using the bodies thus obtained, magnetic fields can then be calculated for them at the surface assuming that magnetization is only induced. Descrepancies between the calculated fields and the observed fields would be due to the contribution from remanent magnetization.

These determinations together with field measurements and laboratory tests on collected samples from exposed Younger Granites would allow comparisons to be made between the remanence of exposed and buried granites.

APPENDIX I

THE MAGNETIC FIELD ON A HORIZONTAL SURFACE DUE TO A BODY OF ARBITRARY SHAPE LYING BELOW THE SURFACE

Consider a body of intensity of magnetization J (components: jx, jy, jz). The magnetic potential, A, at the origin (outside the body) due to a volume element, $\Delta x \Delta Y \Delta Z$, of the body, which has position vector $R_1 (R^2 = x^2 + y^2 + z^2)$, is given by

$$A = \frac{Jx\,X + Jy\,Y + Jz\,Z}{R^3} \Delta x \Delta y \Delta z \quad \text{.....(A.1)}$$

The three components of the magnetic field intensity for the body are:

$$\Delta X = \iiint -\frac{\partial A}{\partial x}\, dxdydz; \quad \Delta Y = \iiint -\frac{\partial A}{\partial y}\, dxdydz;$$

$$\Delta Z = \iiint -\frac{\partial A}{\partial z}\, dxdydz$$

The triple integrals being carried out over the volume of the body. Substituting the value of A form (A.1), and differentiating with respect to X, Y and Z respectively, we get:

$$\left.\begin{aligned} \Delta X &= J_x V_1 + J_y V_2 + J_z V_3 \\ \Delta Y &= J_x V_2 + J_y V_4 + J_z V_5 \\ \Delta Z &= J_x V_3 + J_y V_5 + J_z V_6 \end{aligned}\right\} \text{----------(A.2)}$$

where V_1, V_2, V_3 ---, V_6 represent integrals over the volume of the body given by:

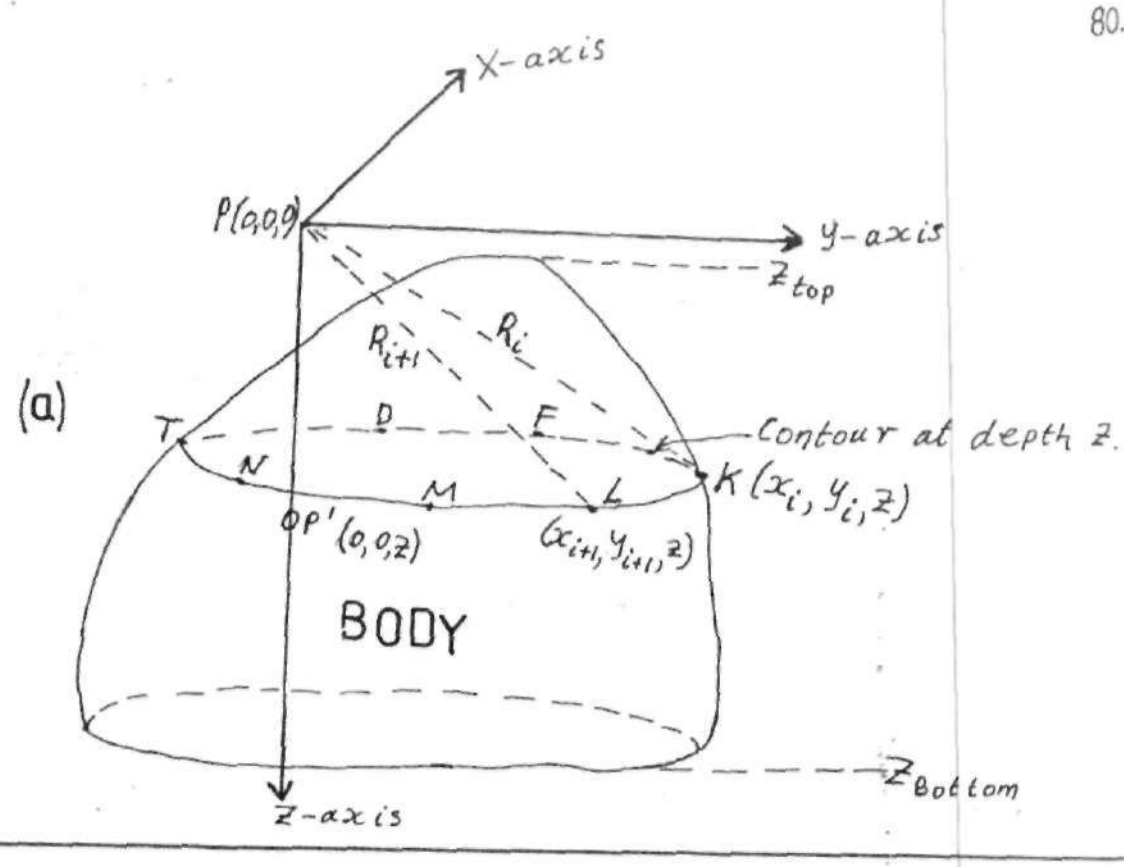


FIG A.1

MODEL BODY SHOWING : (a) A CONTOUR AT DEPTH , and
(b) ITS REPRESENTATION BY A POLYGON

$$V_1 = \iiint \frac{3x^2-R^2}{R^5}\,dx\,dy\,dz \;;\; V_2 = \iiint \frac{3xy}{R^5}\,dx\,dy\,dz$$
$$V_3 = \iiint \frac{3xz}{R^5}\,dx\,dy\,dz \;;\; V_4 = \iiint \frac{3y^2-R^2}{R^5}\,dx\,dy\,dz \qquad \text{--(A.3)}$$
$$V_5 = \iiint \frac{3yz}{R^5}\,dx\,dy\,dz \;;\; V_6 = \iiint \frac{3z^2-R^2}{R^5}\,dx\,dy\,dz$$

In order to evaluate these triple integrals, the method used here performs a double integration analytically and a single integration numerically. The body whose anomaly has to be evaluated is first represented by contours (Fig. A.1). Each contour is then replaced by a polygonal lamina. The double integration is carried out over the surface of each of these horizontal polygonal laminas. The numerical integration is then carried out with respect to the Z-axis. In Fig.A.1 for example, one of the contours has been represented by the polygonal lamina KLMNTDFK. Let the origin P be at the point where the anomaly is being determined and let P^1 lie a distance Z directly below P in the plane of KLMNTDFK. Let the surface part of the volume integrals V_1, V_2, ----, V_6 be denoted by S_1, S_2,----, S_6 respectively,

$$S_1 = \iint \frac{3x^2-R^2}{R^5}\,dx\,dy;\; S_2 = \iint \frac{3xy}{R^5}\,dx\,dy;\; S_3 = \iint \frac{3xz}{R^5}\,dx\,dy$$
$$S_4 = \iint \frac{3y^2-R^2}{R^5}\,dx\,dy;\; S_5 = \iint \frac{3yz}{R^5}\,dx\,dy;\; S_6 = \iint \frac{3z^2-R^2}{R^5}\,dx\,dy$$

$$S_1 = -\sum \frac{\cos^2\theta_i}{Z^2+P_i^2}\left(\frac{g_i\, y_{i+1}-Z^2\tan\theta_i}{R_{i+1}} - \frac{g_i\, y_i - Z^2\tan\theta_i}{R_i}\right)$$

$$S_2 = \sum \frac{\cos^2\theta_i}{Z^2+\rho_i^2}\left(\frac{g_i\, y_{i+1} + g_i^2 + Z^2}{R_{i+1}} - \frac{g_i\, y_i \tan\theta_i + g_i^2 + Z^2}{R_i}\right)$$

$$S_3 = -\sum \frac{\cos^2\theta_i}{Z^2+\rho_i^2}\left(\frac{y_{i+1}\sec^2\theta_i + g_i\tan\theta_i}{R_{i+1}} - \frac{y_i\sec^2\theta_i + g_i\tan\theta_i}{R_i}\right)$$

$$S_4 = \sum \frac{\sin^2\theta_i}{Z^2+\rho_i^2}\left(\frac{C_i X_{i+1} - Z^2\cot\theta_i}{R_{i+1}} - \frac{C_i X_i - Z^2\cot\theta_i}{R_i}\right)$$

$$S_5 = \sum \frac{Z\sin^2\theta_i}{Z^2+\rho_i^2}\left(\frac{X_{i+1}\operatorname{cosec}^2\theta_i + C_i\cot\theta_i}{R_{i+1}} - \frac{X_i\operatorname{cosec}^2\theta_i + C_i\cot\theta_i}{R_i}\right)$$

$$S_6 = -\sum \frac{\rho_i}{Z^2+\rho_i^2}\left(\frac{r_{i+1}\cos\beta_i}{R_{i+1}} - \frac{r_i\cos\beta_i}{R_i}\right) \text{-----(A.4)}$$

The above summations are made for the total number of sides of the polygon. The trigonometrical functions $\tan\theta_i$, $\cot\theta_i$, $\sin\theta_i$, $\sec\theta_i$, $\operatorname{cosec}\theta_i$, $\cos\beta_i$ as well as the intercepts C_i and g_i, and the distances r_i, r_{i+1}, R_i, R_{i+1}, and ρ_i can all be expressed in terms of x_i, y_i, the co-ordinates of K and X_{i+1}, y_{i+1} the co-ordinates of L.

Thus the integrals S_1, S_2, ----, S_6 can all be expressed in closed form in terms of the cartesian co-ordinates of the corners of the polygon.

Finally, V_1, V_2, ----, V_6 are evaluated by performing the numetrical integrals:

$V_1 = \int S_1 dZ$, $V_2 = \int S_2 dz$, $V_3 = \int S_3 dz$,

$V_4 = \int S_4 dz$, $V_5 = \int S_5 dz$, $V_6 = \int S_6 dz$, the limits for each of the integrals are Z top Z bottom. If S_{io}, S_{i1} and S_{i2} are the values of S_i corresponding respectively, to the contours at heights Z_o, Z_i and Z_2 the contribution to V_i by the portion of the body lying between the horizontal planes Z_o and Z_2 is given by

$$V_i = \int_{Z_o}^{Z_2} S_i dz$$

$$= 1/6 \left\{ S_{io} \frac{Z_o - Z_2}{Z_o - Z_1} (3Z_1 - Z_2 - 2Z_o) + S_{i1} \frac{(Z_o - Z_2)^3}{(Z_1 - Z_o)(Z_1 - Z_o)} \right.$$

$$\left. + S_{iz} \frac{Z_o - Z_2}{Z_2 - Z_1} (3Z_1 - Z_o - 2Z_2) \right\} \text{ ----------(A.5)}$$

By choosing successive sets of these point (Z_o, Z_1, Z_2), the numerical quadrature can be carried out throughout the entire range of Z^{1s}, and V_1, V_2, ---, V_6 can be obtained. By shifting the origin to another point and by referring the co-ordinates of all the polygon corners to this point, the values of V_1, V_2, ---, V_6 for any point can be substituted in (A.2) to get the three components of the magnetic anomaly ΔX, ΔY, ΔZ.

When magnetization is taken as being by induction in the earth's field, the total intensity anomally, ΔT, is given by:

$\Delta T = \Delta X \text{Cos D Cos I} + \Delta Y \text{ Sin D Cos I} + \Delta Z \text{ Sin I}$ ------(A.6) where D is magnetic declination, I the inclination. Thus assuring induced magnetization, the magnetization components are given by

$$\left.\begin{aligned} J_x &= J \text{ Cos I Cos D} \\ J_y &= J \text{ Cos I Sin D} \\ J_z &= J \text{ Sin I} \end{aligned}\right\} \text{------(A.7)}$$

and $J = K \cdot Ho$----------(A.8)

where K is the susceptibility and Ho is the earth's magnetic field. Substituting in (A.2) gives ΔT in terms of the magnetization components (J_x, J_y, J_z) as

$$\left.\begin{aligned} \Delta T = Jx\ (V_1 \text{Cos D Cos I} + V_2 \text{ Sin D Cos I} + V_3 \text{ Sin I}) \\ +Jy\ (V_2 \text{Cos D Cos I} + V_4 \text{ Sin D Cos I} + V_5 \text{ Sin I}) \\ +Jz\ (V_3 \text{Cos D Cos I} + V_5 \text{ Sin D Cos I} + V_6 \text{ Sin I}) \end{aligned}\right\} \text{(A.9)}$$

APPENDIX 2

(The Modelling Program)

```
      PROGRAM ptw2 (INPUT, OUTPUT, TAPE 5 = INPUT,
           TAPE 6 = OUTPUT).
C     NP is number of Grid Points
C     NC is number of contours
C     N(J) is number of points on contour J
      AI =  AI * CON
      AD =  AD * CON
      VJ =  SK * F
      DO  1 1  J = 1, NP
11    READ (5, 51) XO(I), YO(I), AN(I)
51    FORMAT
      READ (5, 51) Z(1) .....Z(J)
      DO 12  I = 1, N(J)
12    READ (5, 52) XX (J,I), YY(J,I)
      JX = VJ * COS (AI) * COS (AD)
      JY = VJ * COS (AI) * SIN (AD)
      JZ = VJ * SIN (AI)
c     Variation of parameters begins
        I1  =  1
c     Determination of theoretical Field values
c     k is index of points
c     J is index of contours
      Do 15  K  = 1, NP
      Do 16  J  = 1, NC
```

```
      S1(J)  =  0.0
      S2(J)  =  0.0
      ..............
      S6(J)  =  0.0
      Do 17 I = 1, N(J)
      X(I)   =  XX(J, I) - XO(K)
      Y(I)   =  YY(J, I) - YO(K)
      M1     =  N(J) + 1
      X(M1)  =  X(1)
      Y(M1)  =  Y(1)
7     CONTINUE
      Do 18  I  =  1, N(J)
      MS(I)  =  (Y(I+1)-Y(I))/(X(I+1)-X(I))
      NS(I)  =  1.0/MS(I)
      G(I)   =  X(I)-Y(I) * NS(I)
      C(I)   =  Y(I)-X(I)*MS(I)
      RP(I)  =  SQRT(X(I+1)**2+ Y(I)**2 + Z(J) **2)
      R(I)   =  SQRT(X(I)**2 + Y(I) **2+Z(J) **2)
      RB(I)  =  SQRT((X(I) - X(I+1))**2+(Y(I)-Y(I+1))**2
      P(I)   =  G(I) / (SQRT(1.0 + NS(I) **2))
      R1(I)  =  SQRT (X(I) **2 + Y(I) **2)
      R2(I)  =  SQRT (X(I+1) **2 + Y(I+1) **2)
      CSB(I) =  (X(I)**2-X(I+1)+Y(I)**2-Y(I+1))/(RB(I)*R1(I))
      CSG(I) =  (X(I+1) * (X(I) - X(I+1)) + Y(I+1)
                * (Y(I) - Y(I+1)))/(RB/I)*R2
      BT1    =  (9(I) * Y(I+1) - NS (I) * Z(J)**2)/RP(I)
      BT1    =  BT1-(G(I)*Y(I)-NS(I)*Z(J)**2)/R(I)
```

```
      S1(J) = S1(J)-BT1/(1+NS(I)**2)*(Z(J)**2+P(I)**2))
      BT2   = (9(I)**2+Z(J)**2+G(I)*Y(I+1)*NS(I))/RP(I)
      BT2   = BT2-(G(I)**2+Z(J)**2+G(I)*Y(I)*NS(I))/R(I)
      S2(J) = S2(J) + BT2/((1+NS(I)**2)*(Z(J)**2+P(I)**2))
      BT3   = (Y(I+1)*(1+NS(I)**2)+G(I)*NS(I))/RP(I)
      BT3   = BT3-(Y(I)*(1+NS(I)**2)+G(I)*NS(I)/R(I)
      S3(J) = S3(J)-Z(J)*BT3/((1+NS(I)**2) * (Z(J)**
             2+P**2))
      BT4   = (C(I) * X(I+1) -MS(I) * Z(J)**2)/RP(I)
      BT4   = BT4 - (C(I) * X(I) - MS(I) * Z(J)**2/R(I)
      S4(J) = S4(J)+BT4/((I+MS(I)**2)*(Z(J)**2+P(I)**2))
      BT5   = (X(I+1)*(1+MS(I)**2)+C(I)*MS(I))/RP(I)
      BT5   = BT5-(X(I)*(1+MS(I)**2) + C(I)*MS(I)/R(I)
      S5(J) = S5(J)+BT5*Z(5)/((1+MS(I)**2)*(Z(J)**2
             + P(I) **2))
      BT6   = R2(I)*CSG(I)/RP(I)-R1(I)*CSB(I)/R(I)
      S6(J) = S6(J) - BT6 *P(I)(P(I)**2+Z(J) **2)
   18 CONTINUE
   16 CONTINUE
      UJ    = SJ(1) *(Z(I)-Z(3))*(3.0*Z(2)-Z(3)-Z*Z(1))
             /(Z(I)-Z(2))
      UJ    = UJ+SJ(2)*(Z(1)-Z(3)**3/((Z(2)-Z(3))*
             (Z(2)-Z(1)))
      UJ    = UJ+SJ(3)*(Z(1)-Z(3)*(3*Z(2)-Z(1)
             -Z*Z(3))/(Z(3)-Z(2))
      VJ(K) = UJ/6.0
```

```
      T1 = JX*(V1(K)*COS(AD)*COS(AI)+V2(K)*SIN(AD)
           *COS(AI)+  J3(K) * SIN (AI)
      T2 = JY*(V2  (K)*COS(AI)+ V4(K)*SIN(AD)*COS(AI)+
              V5 (K) * SIN (AI)
      T3 = JZ * ( V3(K) * COS(AD) * COS(AI) +
             V5 (K) * SIN (AI)
      T3 = JZ *( V3(K) * COS (AD) * COS (AI) +
             V5(K)*SIN(AD)*COS(AI)+ 6(K)*SIN(AI)
      DT(K) = T1 + T2 + T3
      DX(K) = AN(K) - DT(K)
15    CONTINUE
C     Calc. of correlation coefficients betwee DT & AN
      SuM X1 = 0.0
      Sum X2 = 0.0
      Sx1SQ  = 0.0
      Sx2SQ  = 0.0
      Sx1x2  = 0.0
      Do 111 K1 = 1,NP
      X1 = DT(KI)
      X2 = AN(KI)
      SUM X1 = SUM X1 + X1
      SUM X2 = SUM X2 + X2
      SX1SQ  = SX1SQ + X1 * X1
      SX2SQ  = SX2SQ + X2 * X2
      SX1X2  = SX1X2 + X1*X2
111   CONTINUE
```

```
      VAR  =  (NP * SX1SQ - SUM X1**2)/(NP*(NP-1))
      STDEV1 = SQRT(VAR)
      VAR = (NP*SX2SQ-SUM X2**2)/(NP*(NP-1))
      STDEV2 = SQRT(VAR)
      COV  =  (NP*SX1X2-SUM X1* SUM X2)/(NP*(NP-1))
      COR  =  COV/(STDEV1 * STDEV 2)
      WRITE (6,661) X1
51    FORMAT
      WRITE (6,661) COR
      DO 305 I = 1, NP
      WRITE (6,661) DX(I)
05    CONTINUE
      STOP
      END
```

R E F E R E N C E S

Ajakaiye, D.E. (1974) - A Gravity Profile across the Banke ring complex, Nigeria Geo-exploration 12, 59-66.

Ajakaiye, D.E., Sweeney J.F. 1974 - Three Dimensional Gravity interpretation of the Dutsen-Wai Complex, Nigerian Younger Granite Province. Tectonophysics 21, 331-341.

Ajakaiye, D.E. 1974 - A Gravity Survey over the Nigerian Younger Granite Province. In "Geology of Nigeria" ed. C.A. Kogbe 207-224.

Ajakaiye, D.E. 1974 - Density of rocks in the Nigerian Younger Granite Province. Journal of Mining Geology 11, 33-43.

Ajakaiye, D.E. - Hall D.H., Miller, T. 1982 - Aeromagnetic Anomalies across the Nigerian Younger Granite Province (IN PRESS).

Baranov V. 1960 - Role des mathematiques dans l'art de l'interpretation. Geophysical Prospecting 8 141-147.

Bhattacharyya B.K. 1964 - Magnetic Anomalies due to Prison-shaped bodies with arbitrary polarization. Geophysics 29, 517-531.

Bhattacharyya B.K. 1965 - Two-dimensional Harmonic analysis as a tool for magnetic interpretation. Geophysics 30, 237-252.

McCraken D.D. 1967 - Fortran with Engineering Applications. John Wiley & Sons Inc.

Davis, J. C. 1976 - Statistics and Data Analysis in Geology. John Wiley & Sons

Dobrin, M. B. 1976 - Introduction to Geophysical Prospecting McGraw Hill Book Co., Inc.

Elsasser, W.M. 1958 - The Earth as a Dynamo Scientific American Inc. 1958.

Flint R.F., Skinner B.J. 1977 - Physical Geology John Wiley & Sons, Inc. 1977

Grant F.S., West G.F., 1965 - Interpretation Theory in Applied Geophysics. McGraw-Hill Book Co., Inc. 1965.

MacLeod W.N., Turner D.C., Wright E.P. 1971. The General Geology of the Jos Plateau Vol. 1 General Geoloty Bul. Geol. Surv. Nig. 32.

MacGrath P.H., Hood P.J. 1970 - The dipping dike case: A Computer curve matching method of magnetic interpretation - Geophysics 35, 831-848.

Nettleton, L.L. 1976 - Gravity and Magnetics in Oil Prospecting - McGraw-Hill, Inc. 1976.

Parkinson, W.D. 1982 - Introduction to Geomagnetism Elsevier Science Publishing Co., Inc. 1982

Reford M.S., Summer J.S. 1964 - Aeromagnetics - a review article. Geophysics 29, 482-561.

Regan R.D., Cain J.C. 1975 - The use of Geomagnetic field models in Magnetic Surveys. Geophysics 40.

Robson, D.A. and Green, A.G. 1980 - A magnetic survey of the cureole around the Cheriol granite. Scottish Journal of Geology 16, 11-27.

Royer, G., Naudy, H., Thomas, J., Dryer, H. 1972 Recent Developments in the Acquisition, Processing and Interpretation of High sensitivity Aeromagnetic Data. Bulletin of the "Compagnie Generale de Geophysique".

Shurbet D.H., Keller G.R., Friess, J.P. 1976 Remanent Magnetization from comparison of Gravity and Magnetic Anomalies. Geophysics 41 1323-1347.

Talwani, M. 1965 - Computation with the help of a Digital Computer of Magnetic Anomalies caused by bodies of arbitrary shape. Gephysics 30, 797-817.

Telford, W.M., Geldart L.P., Sheriff R.E., Keys D.A. 1980 - Applied Geophysics. Cambridge University Press 1980.

Turner, D.C. 1974 - Structure and Petrology of the Younger Granite ring complexes. In "Geology of Nigeria" ed. C.A. Kogbe 143-158.

Wright, J.B. 1974 - Volcanic Rocks of Nigeria. In "Geology of Nigeria" ed. C.A. Kogbe 93-143.